Internal solitons in laboratory experiments: Comparison with theoretical models

L. A. Ostrovsky
Zel Technologies/NOAA Environmental Research Laboratory, Boulder, Colorado
and Institute of Applied Physics, Russian Academy of Sciences, Nizhni Novgorod, Russia

Y. A. Stepanyants[a)]
Institute of Applied Physics, Russian Academy of Sciences, Nizhni Novgorod, Russia
and Australian Nuclear Science and Technology Organization, Menai (Sydney), Australia

(Received 4 May 2005; accepted 14 September 2005; published online 21 October 2005)

Nonlinear internal solitary waves observed in laboratory experiments are discussed from the standpoint of their relation to different soliton theories, from the classical integrable models such as the Korteweg–de Vries, Gardner, Benjamin–Ono, and Joseph–Kubota–Ko–Dobbs equations and their modifications, through the nonintegrable models describing higher-order nonlinear effects, viscosity, rotation, and cylindrical spreading, to the strongly nonlinear models. First, these theoretical models are briefly described and, then, laboratory data and their comparison with the theory are presented. © *2005 American Institute of Physics*. [DOI: 10.1063/1.2107087]

Internal solitary waves probably comprise the most ubiquitous type of solitons existing in a natural environment. They are regularly observed in oceans and often in the atmosphere. Numerous experimental studies of internal solitons in laboratory tanks have been performed in the last few decades. Such experiments provide detailed quantitative information usually unavailable in field conditions, and they are also an efficient tool for verifying numerous theoretical models. In this paper we present a review of studies of internal solitons in laboratory tanks and a discussion of the relationship between experimental results and the existing theoretical models, including both the well-known integrable equations and the less thoroughly studied nonintegrable models, taking into account such factors as dissipation, rotation, cylindrical divergence, and strong nonlinearity.

I. INTRODUCTION

The importance of laboratory observations of internal solitary waves (or internal solitons; we shall not distinguish between these two terms) has been appreciated since the mid-20th century, although researchers have studied internal waves in laboratory experiments since the beginning of the 20th century, after the famous cruise by Fridtjof Nansen to the North Pole onboard the ship "Fram" (1893–1896). It is worth noting, however, that Benjamin Franklin, one of the Founding Fathers of America, was apparently the first who described the observation of internal waves in the "laboratory conditions"[1] (the authors thank Yu. D. Chashechkin for this reference). During his oceanic voyage from Madeira to America, he observed that the interface between oil and water in his self-made lamp was "in great commotion, rising and falling in irregular waves," while "the surface of the oil was perfectly tranquil, and duly preserved its position and distance with regard to the brim of the glass." Since his arrival in America, Franklin "repeated the experiment frequently" at home with the model of the lamp containing the same two-layer fluids, water, and oil. Then, he amused himself by showing this experiment "to a number of ingenious persons" and wrote to his friend, Sir John Pringle, "those who are but slightly acquainted with the principles of hydrostatics, &c. are apt to fancy immediately that they understand it, and readily attempt to explain it; but their explanation have been different, and to me not very intelligible."

Purposeful laboratory experiments with internal solitons were conducted practically in parallel with the development of theoretical models and active field studies of internal waves after the Second World War. The first simplified models either known by or developed in that time were mainly integrable models. They include equations now known as classical: the Korteweg–de Vries (KdV), Gardner [also known as the extended Korteweg–de Vries (eKdV) equation] Benjamin–Ono (BO), Joseph–Kubota–Ko–Dobbs (JKKD) equations, and others (see, e.g., Ref. 2).

Numerous experiments conducted with both surface and internal waves in laboratory tanks have demonstrated that solitons emerge easily from initial perturbations; they can be readily registered and their properties can be studied in detail and compared with theoretical predictions. Currently, it is a widely accepted view that solitons (or at least structures close to solitary waves) exist as ubiquitous features in oceans and in the atmosphere, and that they can be observed at hundreds of locations around the globe. However, in natural conditions experimentalists can register usually only solitary waves and roughly measure only few of their characteristics, whereas in the laboratory, it is possible to control the parameters of solitons and study their properties in great detail.

In this review paper we briefly outline some known integrable and nonintegrable theoretical models of internal solitons, including recently developed, strongly nonlinear

[a)]Corresponding author. Electronic mail: Yury.Stepanyants@ansto.gov.au

models and models accounting for fluid rotation. Then we give a summary of laboratory experiments available in the literature and compare their results with theoretical predictions. In the Conclusions we discuss the main outcomes of existing laboratory experiments.

II. INTEGRABLE WEAKLY NONLINEAR MODELS OF INTERNAL WAVES

Until now, the majority of relevant laboratory experiments have dealt with verifying weakly nonlinear, long-wave integrable models such as KdV, BO, JKKD, and their modifications. We begin with a brief list of the well-known equations considered as basic in laboratory experiments. They deal with moderate-amplitude waves for which the velocity variations in the wave are small compared with the wave phase velocity. Also, the characteristic wavelength is assumed to be large compared with the characteristic vertical scale of the problem. Nonintegrable models, including those of strongly nonlinear processes, will be addressed further later in this paper.

Many equations in question follow from a modal representation. In particular, vertical velocity w and horizontal velocity vector $\mathbf{U}$ are represented by an expansion in eigenmodes:

$$w = \sum_{m=1}^{\infty} W_m(z) w_m(x,y,t), \quad \mathbf{u} = \sum_{m=1}^{\infty} C_m \frac{dW_m}{dz} \mathbf{U}_m(x,y,t); \tag{1}$$

and the vertical displacement of the isopycnal surfaces (the surfaces of equal density) is given by $\xi(x,y,z,t) = \Sigma_{m=1}^{\infty} \eta_m(x,y,t) W_m(z)$, and similarly for other variables. Here C_m are constants. The orthogonal eigenfunctions W_m satisfy the boundary-value problem in the linear, nondispersive approximation:

$$\frac{d}{dz}\left(\rho(z)\frac{dW}{dz}\right) + \frac{\rho(z)N^2(z)}{c^2} W = 0. \tag{2}$$

Here $N(z) = \sqrt{-(g/\rho)d\rho/dz}$ is the Brunt–Väisälä (buoyancy) frequency, g is the gravity acceleration, and $\rho(z)$ is the static water density.

With the appropriate boundary conditions at the bottom, $W(-H)=0$, and the water surface, $W(0)=\partial\xi_s/\partial t$, where ξ_s is surface displacement, the eigenfunctions W_m and eigenvalues $c=c_m$ $(m=1,2,3,\ldots)$ can be found with c_m being the long-wave velocity for the corresponding mode. After substituting these expansions into the hydrodynamic equations and retaining only one, mth mode, the equations for horizontal variations follow in which dispersive and nonlinear terms are assumed to be small. In general, they are two-directional equations (known as Boussinesq equations in nonlinear wave theory, and should not be confused with Boussinesq equations in shallow water theory); the next step is a transition to one-directional (KdV-type) equations describing progressive waves. The corresponding derivation can be found in different textbooks (see, e.g., 3 and 4); here we only give a few relevant results. (Note that Boussinesq equations for internal waves analogous to those known as classical Boussinesq equations for surface waves were apparently presented for the first time in Ref. 5.)

At small density variations, which are always the case in the ocean and often in the laboratory (see the data below), this boundary-value problem is simplified by applying the "rigid lid" approximation, $W(0)=0$, applying the Boussinesq approximation when the variations of water density, ρ, are neglected everywhere except in the buoyancy frequency.

A. Korteweg–de Vries (KdV) equation

For a progressive wave propagating, with certainty, in the positive direction of axis x, the classical KdV equation widely discussed in the literature has the form

$$\frac{\partial\eta}{\partial t} + c\frac{\partial\eta}{\partial x} + \alpha\eta\frac{\partial\eta}{\partial x} + \beta\frac{\partial^3\eta}{\partial x^3} = 0, \tag{3}$$

where the nonlinearity and dispersion parameters (α and β, respectively) are

$$\alpha = \frac{3c\sigma}{2H}, \quad \beta = \frac{c\,DH^2}{2}, \tag{4}$$

with σ and D given in the general case by (see, e.g., Ref. 6 and references therein)

$$\sigma = \frac{H}{Q}\int_{-H}^{0} \rho(z)\left(\frac{dW}{dz}\right)^3 dz, \quad D = \frac{1}{H^2 Q}\int_{-H}^{0} \rho(z) W^2 dz,$$
$$Q = \int_{-H}^{0} \rho(z)\left(\frac{dW}{dz}\right)^2 dz. \tag{5}$$

Here $\rho(z)$ is the density profile in the fluid layer; $W(z)$ is the eigenfunction for the corresponding m-th mode found from the boundary-value problem (2) in the limit of infinitely long waves, and H is the total fluid depth (for details see, e.g., 4, 6, and 7).

The well-known solitary solution to Eq. (3) is

$$\eta(x,t) = \eta_0 \operatorname{sech}^2 \frac{x - Vt}{\Delta}. \tag{6}$$

The nonlinear velocity V and characteristic width Δ of this soliton are related to the linear speed c and the amplitude of the displacement η_0 by

$$V = c + \frac{\alpha\eta_0}{3}, \quad \Delta^2 = \frac{12\beta}{\alpha\eta_0}. \tag{7}$$

The dispersion parameter β is always positive for gravity waves, whereas for capillary waves on a surface of thin liquid film this parameter may be negative. The nonlinear parameter α may be both positive and negative. The combination of parameters α and β determines the soliton polarity; namely, the sign of η_0 is such that Δ^2 in Eq. (7) is positive. Thus, if α is negative, η_0 also will be negative, i.e., for instance, the soliton on the interface of a two-layer fluid is a depression.

An important limiting case is the two-layer model with thicknesses of the upper and lower layers of h_1 and h_2, respectively. The fluid density is $\rho=\rho_1$ for $0>z>-h_1$ and $\rho=\rho_2>\rho_1$ for $-h_1>z>-H$, where $H=h_1+h_2$ is the total depth. In this case the coefficients c, α, and β can be calcu-

lated in the explicit form. In the case of a rigid lid boundary condition on the surface of the upper fluid, the coefficients are (see, e.g., Ref. 6 and references therein)

$$c = \left(\frac{g(\rho_2 - \rho_1) h_1 h_2}{\rho_2 h_1 + \rho_1 h_2} \right)^{1/2} \simeq \left(\frac{g\, \delta\rho}{\rho} \frac{h_1 h_2}{h_1 + h_2} \right)^{1/2}, \tag{8}$$

$$\alpha = \frac{3c}{2 h_1 h_2} \frac{\rho_2 h_1^2 - \rho_1 h_2^2}{\rho_2 h_1 + \rho_1 h_2} \simeq \frac{3}{2} c \frac{h_1 - h_2}{h_1 h_2}, \tag{9}$$

$$\beta = \frac{c h_1 h_2}{6} \frac{\rho_1 h_1 + \rho_2 h_2}{\rho_2 h_1 + \rho_1 h_2} \simeq \frac{c h_1 h_2}{6}. \tag{10}$$

The relations on the right are valid for those cases when $\delta\rho = \rho_2 - \rho_1$ is small relative to the density of the layers ($\delta\rho/\rho_2 \ll 1$); which is important, in particular, for the modeling of oceanic conditions. In the case of a free surface boundary conditions, only small corrections to the coefficients c and β usually arise, whereas the coefficient α becomes more complex[8–10] (this is discussed in more detail in Sec. II B).

A slightly more general solitary wave solution was obtained by Keulegan[11] for the Boussinesq equation describing interfacial waves propagating in opposite directions in the two-layer model. The Keulegan's soliton has the same sech^2 profile as the KdV soliton (6), but with slightly different relationships between the amplitude, η_0, velocity, V, and half-width, Δ:

$$V = c \sqrt{1 + \frac{h_1 - h_2}{h_1 h_2} \eta_0}, \quad \Delta^2 = \frac{4}{3} \frac{h_1^2 h_2^2}{(h_1 - h_2)\eta_0}. \tag{11}$$

In the limit of $\eta_0 \to 0$ these formulas reduce to the corresponding expressions (7) for the KdV soliton.

B. The extended Korteweg–de Vries (Gardner) equation

An interesting situation arises when the nonlinear coefficient α is small or even equal to zero. The condition of the vanishing of nonlinear coefficient α depends on boundary conditions. As follows from Eq. (9), in the case of a rigid lid approximation, there is a simple relationship between the critical depth ratio $b \equiv h_1/h_2$ and density ratio $a \equiv \rho_1/\rho_2$ that provides $\alpha = 0$: $b_{\rm cr} = \sqrt{a}$ (in the Boussinesq approximation $b_{\rm cr} = 1$). In the case of a free surface, the critical depth ratio can be found as the real root of the cubic equation[8,9]

$$b^3 + (a^2 + 3a - 3)b^2 + (3 - 4a)b - 1 = 0, \tag{12}$$

which is

$$b_{\rm cr} = \sqrt[3]{\frac{a}{54}} [S_p(a) + S_m(a)] + 1 - a - \frac{a^2}{3}, \tag{13}$$

where $S_{p,m}(a) = [27 + 27a + 18a^2 - 36a^3 - 18a^4 - 2a^5 \pm 3(1+2a) \times \sqrt{3(1-a)(27+5a)}]^{1/3}$.

The comparison of these two cases is presented in Fig. 1. As one can see, both dependencies $b_{\rm cr}(a)$ agree only when $a \to 1$, i.e., when the Boussinesq approximation is valid.

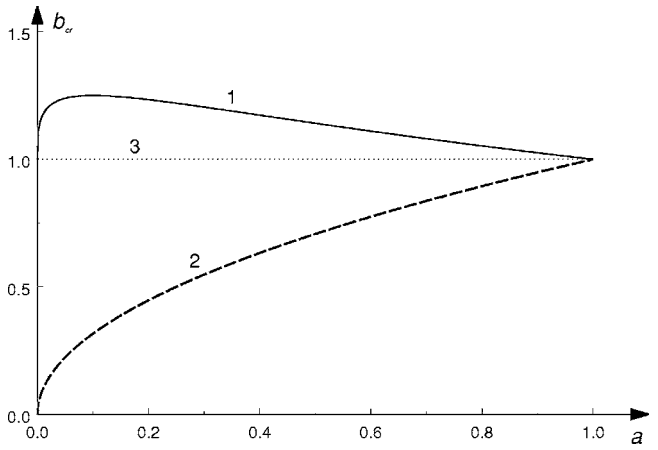

FIG. 1. Dependency of the critical depth ratio $b_{\rm cr} = (h_1/h_2)_{\rm cr}$ on density ratio $a = \rho_1/\rho_2$ for free surface (line 1) and rigid lid approximation (line 2); line 3 represents a critical depth ratio within the framework of the Boussinesq approximation, i.e., when $\rho_1 \approx \rho_2$.

Meanwhile, at smaller values of a, they are quite different: in the case of a free surface $b_{\rm cr} > 1$, whereas in the case of a fluid under the rigid lid $b_{\rm cr} < 1$.

When the nonlinear coefficient α becomes anomalously small or vanishes, one must take into account higher-order nonlinear terms in the evolution equations. In the latter case, the extended Korteweg–de Vries (eKdV) equation (also called the combined KdV and Gardner equation), having both quadratic and cubic nonlinearities, results in

$$\frac{\partial \eta}{\partial t} + (c + \alpha\eta + \alpha_1 \eta^2) \frac{\partial \eta}{\partial x} + \beta \frac{\partial^3 \eta}{\partial x^3} = 0, \tag{14}$$

where in the case of a two-layer fluid with a rigid lid, the second nonlinear coefficient is (see, e.g., Ref. 6 and references therein)

$$\alpha_1 = \frac{3c}{h_1^2 h_2^2} \left[\frac{7}{8} \left(\frac{\rho_2 h_1^2 - \rho_1 h_2^2}{\rho_2 h_1 + \rho_1 h_2} \right)^2 - \frac{\rho_2 h_1^3 + \rho_1 h_2^3}{\rho_2 h_1 + \rho_1 h_2} \right] \simeq -\frac{3}{8} c \frac{(h_1 + h_2)^2 + 4 h_1 h_2}{h_1^2 h_2^2}. \tag{15}$$

The last expression is again valid for the case of close densities. As follows from Eq. (15), within the framework of a two-layer model, the coefficient α_1 is always negative. However, in the general case α_1 may be both negative and positive depending on the density stratification and shear-flow profile.[12,13]

The form of soliton solutions of Eq. (14) depends on the sign of coefficient α_1. In the case of negative α_1, the soliton solution can be written in the form of a stationary moving kink–antikink pair:

$$\eta(x,t) = -\frac{\alpha}{\alpha_1} \frac{\nu}{2} \left[\tanh\left(\frac{x - Vt}{\Delta} + \phi \right) - \tanh\left(\frac{x - Vt}{\Delta} - \phi \right) \right], \tag{16}$$

where ν is a free dimensionless parameter with the range $0 < \nu < 1$, and the remaining parameters are

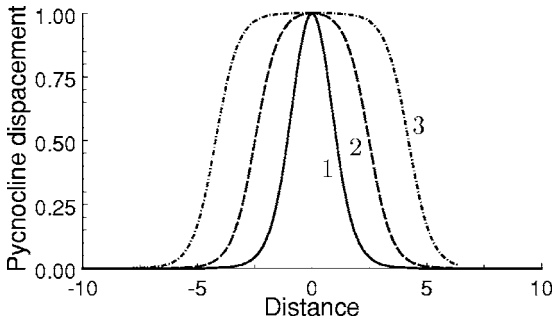

FIG. 2. Normalized wave shapes in the eKdV equation (16) for three values of parameter $\varepsilon=1-\nu$: 1—$\varepsilon=10^{-1}$ (close to the KdV case); 2—$\varepsilon=10^{-4}$; 3—$\varepsilon=10^{-7}$.

$$\phi(\nu)=\frac{1}{4}\ln\left(\frac{1+\nu}{1-\nu}\right),\quad \Delta=\sqrt{\frac{-24\alpha_1\beta}{\alpha^2\nu^2}},\quad V=c-\frac{\alpha^2\nu^2}{6\alpha_1}. \tag{17}$$

Figure 2 shows the normalized shapes of eKdV solitons for three values of parameter ν. Similar to the KdV soliton, the velocity of this eKdV soliton is always greater than the velocity c of long linear waves. The amplitude of the soliton $\eta_0=|\alpha/\alpha_1|\nu\tanh\phi$ varies from zero at $\nu=0$ to the maximum of

$$\left(\frac{\eta_0}{h_2}\right)_{\max}=\left|\frac{\alpha}{\alpha_1 h_2}\right|=\frac{4b|b^2-a|}{b^4+2ab(4b^2+7b+4)+a^2}, \tag{18}$$

at $\nu=1$, where $a=\rho_1/\rho_2$ and $b=h_1/h_2$. In contrast to the KdV soliton, which can, in principle, vary in amplitude from zero to infinity, the eKdV soliton amplitudes are always restricted from above by that value. When the eKdV soliton approaches maximum, its width increases so that the soliton profile changes from a bell shape to a rectangular shape representing a kink–antikink pair described by Eq. (16). In the limit $\nu\to 1$, the eKdV soliton transforms into infinitely separated kink and antikink.

In the near-critical situation when $b\to\sqrt{a}$ and the quadratic nonlinear coefficient is small, the eKdV equation is indeed applicable. The maxima of the soliton amplitude and velocity are given by

$$\left(\frac{\eta_0}{h_2}\right)_{\max}\approx\frac{|b-\sqrt{a}|}{1+\sqrt{a}}, \tag{19}$$

$$V_{\max}=c-\frac{\alpha^2}{6\alpha_1}=c\left(1+\frac{(b^2-a)^2}{b^4+2ab(4b^2+7b+4)+a^2}\right)\underset{b\to\sqrt{a}}{\approx}c\left(1+\frac{(b-\sqrt{a})^2}{2\sqrt{a}(1+\sqrt{a})^2}\right). \tag{20}$$

The limiting-amplitude soliton corresponds to the case when its crest is exactly at the critical depth (in the Boussinesq fluid it is at the mid-depth). From Eq. (17) it follows that, in general,

$$\eta_0=-\frac{\alpha\nu}{\alpha_1}\frac{\sqrt{1+\nu}-\sqrt{1-\nu}}{\sqrt{1+\nu}+\sqrt{1+\nu}}, \tag{21}$$

with ν related to ϕ and Δ by Eqs. (17).

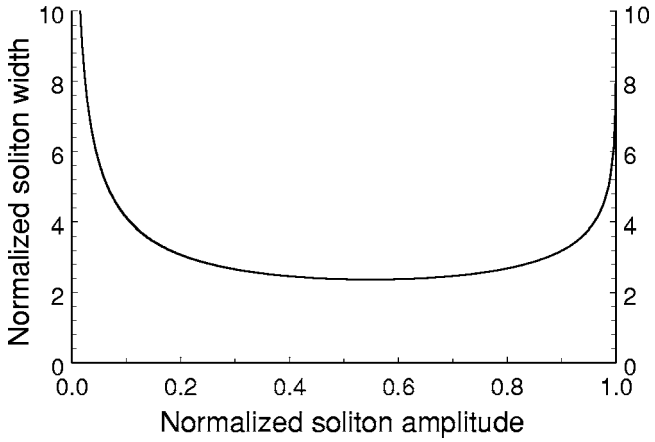

FIG. 3. Dependency of the characteristic width, $\bar{D}_{0.5}$, of eKdV solitons, Eq. (16), on amplitude $\bar{\eta}_0$ in dimensionless variables: $\bar{D}_{0.5}=D_{0.5}|\alpha|/(24\alpha_1\beta)^{1/2}$; $\bar{\eta}_0=\eta_0\alpha_1/\alpha$.

The width of the soliton increases in both limits: $\nu\to 0$ and $\nu\to 1$. Hence, for some $\nu=\nu_m$ there exists a minimum value of D. Figure 3 depicts $D_{0.5}$, the full width of the soliton at half its maximum amplitude, as a function of amplitude, η_0. The minimum of $D_{0.5}$ occurs at $\nu\approx 0.9$, when the amplitude is about 0.56 of the maximum. A more detailed discussion of the dependency between D and η_0 both for weakly nonlinear perturbations, described by the eKdV equation, and for more intensive perturbations, described by the primitive Eulerian equations, can be found in Ref. 14.

Although the eKdV equation is valid for small nonlinearity, it can sometimes be successfully applied to the description of strongly nonlinear internal solitons as a phenomenological model, whereas the usual KdV equation fails to approximate observational and laboratory data. The reason for this is a qualitative (but, in general, not quantitative) correspondence of the eKdV solitons to strongly nonlinear solitary waves in a two-layer fluid in what is regarding a nonmonotonous dependency of their width on the amplitude and the existence of limiting amplitude.

In the conclusion of this section, we mention a situation in which the cubic nonlinear coefficient, α_1, is positive. Such an option can be realized, e.g., in a three-layer fluid.[12,13] A family of possible soliton solutions to the eKdV equation is much richer in this case; it includes solitons of positive and negative amplitudes, algebraic solitons similar to BO solitons (see below), and breathers—nonstationary solitons periodically oscillating in time. They have not been studied in laboratory experiments thus far; meanwhile, a theory predicts their existence both in laboratory and in natural oceanic conditions as well.[15] Further study of these phenomena is a challenge for experimentalists.

C. The Benjamin–Ono (BO) equation

If the wavelength is large compared with one (say, upper) layer but small compared with the other (lower) layer of the ocean, one can let $h_2\to\infty$. These waves may then be described by the differential-integral BO equation:

$$\frac{\partial \eta}{\partial t} + c\frac{\partial \eta}{\partial x} + \alpha\eta\frac{\partial \eta}{\partial x} + \frac{\beta}{\pi}\frac{\partial^2}{\partial x^2}\wp\int_{-\infty}^{\infty}\frac{\eta(x',t)}{x-x'}dx' = 0, \qquad (22)$$

where the symbol $\wp$ indicates that the principal value of the integral should be taken, and the coefficients are

$$c = \sqrt{\frac{(\rho_2-\rho_1)gh_1}{\rho_1}}, \quad \alpha = -\frac{3}{2}\frac{c}{h_1}, \quad \beta = \frac{ch_1}{2}\frac{\rho_2}{\rho_1}. \qquad (23)$$

"Algebraic" solitons described by this equation are also well known:

$$\eta(x,t) = \frac{\eta_0}{1+(x-Vt)^2/\Delta^2}. \qquad (24)$$

Their amplitudes η_0, velocities V, and half-widths Δ are related by

$$V = c + \frac{\alpha\eta_0}{4} \text{ and } \Delta = \frac{4\beta}{\alpha\eta_0}. \qquad (25)$$

The displacement caused by these solitons is the downgoing motion of the pycnocline (sharp density interface) when the upper layer is thin, and, conversely, for the case when the thin layer lies near the bottom (there is a general rule of thumb: pycnocline displacement induced by a soliton is directed to the deepest layer).

D. The Joseph–Kubota–Ko–Dobbs (JKKD) equation

In this case, the thickness of one of the layers, say h_1, is assumed to be small in comparison with the thickness of another, h_2, i.e., $h_1/h_2 \ll 1$. At the same time, the perturbation wavelength, $\lambda \gg h_1$, may have an arbitrary relationship with h_2, i.e., the total water layer can be either shallow or deep. The resulting evolution equation can be presented in a variety of equivalent forms; one of the simplest is

$$\frac{\partial \eta}{\partial t} + c\frac{\partial \eta}{\partial x} + \alpha\eta\frac{\partial \eta}{\partial x} - \beta\frac{\partial^2}{\partial x^2}\wp\int_{-\infty}^{\infty}\frac{\eta(x'/h_2,t)}{\tanh\left(\frac{\pi}{2}\frac{x-x'}{h_2}\right)}dx' = 0, \qquad (26)$$

where, for the two-layer model with a sharp density interface, the parameters c and α are the same as in Eq. (22), and $\beta=(c/4)(h_1/h_2)$.

The JKKD equation has a solitary solution that has been obtained by many authors and presented in different forms. One of the forms convenient for practical applications is

$$\eta(x,t) = \frac{\eta_0\left(1+\cos\frac{2h_2}{\Delta}\right)}{1+\cos\frac{2h_2}{\Delta}+2\sinh^2\frac{x-Vt}{\Delta}}, \qquad (27)$$

where

$$\eta_0 = \frac{4}{3}\frac{h_1^2}{\Delta}\frac{\sin\frac{2h_2}{\Delta}}{1+\cos\frac{2h_2}{\Delta}}, \quad V = c\left(1-\frac{h_1}{\Delta\tan\frac{2h_2}{\Delta}}\right). \qquad (28)$$

Here Δ is a free parameter characterizing the soliton width.

Equation (26) tends to the KdV and BO equations in the limits of $h_2/\Delta \to 0$ at fixed h_1/h_2 and $h_2 \to \infty$, respectively. The same is true for the solutions (27) and (28) in the KdV limit, although the analytical transition to the BO limit for this soliton is not completely clear yet.

The main features of the initial perturbation dynamics within the framework of the JKKD equation are very similar to those described by the KdV model.

All the models listed above have been proven fully integrable, possessing an infinite set of conservation laws and exact multisoliton solutions (see, e.g., Ref. 2). Their properties have been thoroughly studied by mathematicians. However, real wave processes even in controlled laboratory conditions do not obey these equations exactly. Some additional effects such as viscosity, inhomogeneity, effects of strong nonlinearity, and higher-order dispersion, etc., must be taken into account; they lead to nonintegrable models that can be studied by means of approximate or numerical methods.

III. LABORATORY EXPERIMENTS EXAMINING INTEGRABLE MODELS

There is already a plethora of papers in which results from laboratory experiments on internal solitary waves relevant to weakly nonlinear integrable models were published. In general, the results of these experiments are in agreement with the theories outlined above, provided the corresponding conditions are met. At the same time, in many cases noticeable discrepancies have been observed, making it necessary to discuss their possible nature and causes.

One of the earliest experimental observations of internal solitary waves in a laboratory was published by Davis and Acrivos in 1967.[16] A typical sketch of the laboratory setup used in that and subsequent experiments is shown in Fig. 4. The authors dealt with the second (varicose or sausage-type) mode internal wave propagating on a thin pycnocline of relatively deep water. Qualitatively, the shape of a second-mode solitary wave is shown in Fig. 5, taken from the paper by Kao and Pao.[17] It is curious to note that such an experiment was conducted for a deep water configuration before the classical internal KdV solitons in shallow water were observed and even before the Benjamin–Ono equation (22) was derived. Actually, Davis and Acrivos developed their own approximate analytical theory and conducted numerical calculations that describe solitary waves in a thin stratified layer between two thick layers of uniform fluid. They also carried out a laboratory experiment in a tank 250 cm long, 10 cm wide and 40 cm deep (hereafter, the dimensions of other tanks will be indicated in the same order: length $\times$ width $\times$ depth). The tank was half-filled with a uniform solution of saltwater with a density ranging from 1.0 to 1.17 g/cm^3 and then, topped off by freshwater with a density of 1.0 g/cm^3 with a smoothly stratified intermediate layer of 1 cm thickness .

The authors observed stationary solitary waves that were later named Benjamin–Ono (BO) or algebraic solitons. In their experiment wave amplitudes vary in a wide range from small to large. They measured the dependency of soliton ve-

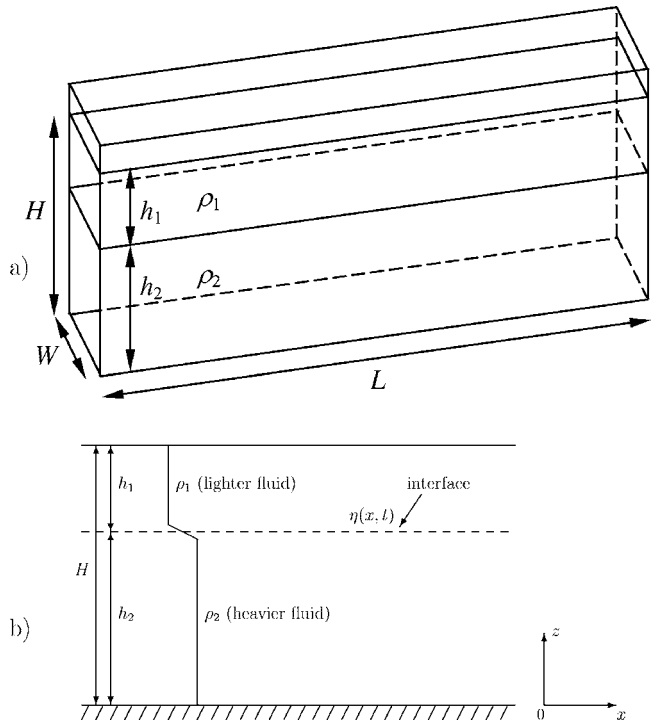

FIG. 4. Sketch of the typical laboratory setup (a) and two-layer fluid configuration (b) used in laboratory studies of internal solitary waves.

locity on amplitude and found rather good agreement with theoretical and numerical predictions for small- and moderate-amplitude solitary waves. For large-amplitude waves the discrepancy between experimental data and the weakly nonlinear theory was quite noticeable. Some asymmetry of wave profiles with respect to the mid pycnocline level clearly can be seen from the photos presented in Ref. 16 both for small- and large-amplitude waves.

Davis and Acrivos also discovered large-amplitude quasistationary solitary formations containing vortex cores with water trapped inside. The trapping occurred within closed streamlines when the amplitude of perturbation exceeded the

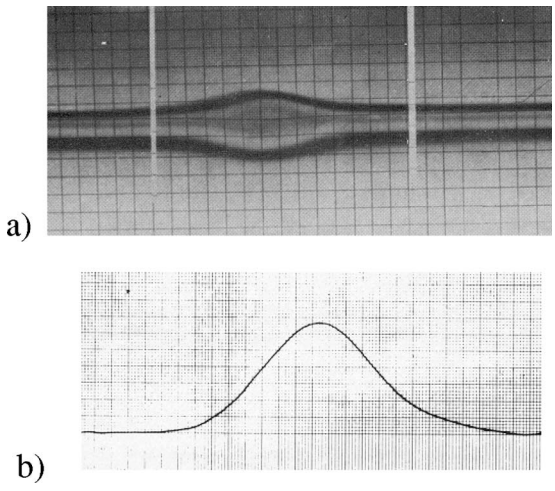

FIG. 5. (a) Photograph of the second-mode solitary wave shape. Interface displacements in a three-layer fluid are visible due to a dye floating at the interfaces (the grid in the photo has a 1 in. spacing). (b) Temporal record of the wave form as measured by the hot-film probe. From Ref. 17.

pycnocline thickness more than 1.2 times. Although no quantitative data were presented for such a strongly nonlinear perturbation, these results demonstrated for the first time that large-amplitude wave-vortex formations (billows) are possible in stratified fluids. They were studied later by other authors whose results are discussed in Sec. V C.

Further, we outline the experiments, which, to a certain degree, were intended to verify shallow-water models, the KdV equation, and its modifications. One of the earliest papers containing detailed quantitative data on KdV solitons was published in 1973 by Walker.[8] This work is characteristic in that, on the one hand, the author claimed that the behavior of observed solitary waves "is generally consistent with that predicted by the Korteweg–de Vries equation." On the other hand, a pronounced deviation of measured solitary wave parameters from theoretical predictions has been detected. Corrections for viscosity improve the situation but do not solve the discrepancy problem completely. In this section we describe only the part of Walker's experiment that somehow agrees with the predictions of the inviscid KdV model. The influence of viscosity will be considered in the following section which deals with experiments with nonintegrable models.

The laboratory tank used in these experiments was 180.8 cm long, 53.7 cm wide, and 11.5 cm deep; the actual working depth was only 5.5 cm. Two immiscible fluids were used, water of density $\rho_2=1$ g/cm^3 on the bottom layer and Varsol I (Humble Oil) of density $\rho_1=0.784$ g/cm^3 on the upper layer. Surface tension at the interface is a strong function of the contact time of the fluids due to mutual solvability. It varied from 40 dyn/cm for freshly mixed fluids to 25 dyn/cm after a one-hour-long contact. The thickness of the lower layer, $h_2=1$ cm, was fixed, whereas different thicknesses of the upper layer were used, $h_1=2,0$; 1.25; 1.1; 0.875; and 0.75 cm. Surface tension was taken into account in evaluation of the KdV nonlinearity and dispersion coefficients, α and β, respectively (note that for surface waves, these coefficients were evaluated already by Korteweg and de Vries in their classical paper of 1895).

Interfacial wave amplitudes in Walker's experiment were "chosen to be as small as possible consistent with good signal-to-noise ratios," so that the small-amplitude approximation that warranties the applicability of the KdV model was well justified. The density difference of two fluids, $\delta\rho=\rho_2-\rho_1=0.216$ g/cm^3, was fairly significant; therefore, a critical depth when the nonlinear coefficient α in the KdV equation vanishes is not predicted well by a theory based on the rigid lid approximation. Instead, more general kinematic and dynamic boundary conditions on a free surface were used.

In Walker's experiments, both elevation and depression solitary waves were observed at the interface depending on depth layer ratios in accordance with the theoretical prediction for fluid with a free surface. The author compared the wave form in the frontal part of the perturbation with different trial functions and found that the agreement with the sech^2 function is the best despite the decay of the solitary waves in the process of propagation due to viscosity. Nevertheless, the author noticed that there was "a small

(<5% in half-width) systematic departure from the sech^2 shape for small waves, with those of elevation being steepened in front and broadened in back, and *vice versa* for those of depression." Because the laboratory tank had a relatively small size and the depths of the layers were also small, the viscous effects played a noticeable role, affecting the results obtained. They are discussed in the subsequent section.

Another experimental study of solitary waves in laboratory conditions was published by Kao and Pao.[17] They dealt with a second-mode solitary wave generated in a three-layer liquid. In these experiments a tank of 796 cm $\times$ 35.6 cm $\times$ 61 cm was filled with a layer of saltwater at the bottom and an equal-depth layer of freshwater on the top. Before pouring the freshwater, three thin dyed layers of intermediate density were poured so that the pycnocline was located at mid-depth (i.e., $h_1=h_2=30.5$ cm) and had a thickness of about 5 cm. Note that in such a hydrological configuration, the quadratic nonlinear coefficient α in the KdV equation is zero for the first mode of the internal waves (see the previous). The authors considered the second mode for a continuously distributed density profile fitted by a hyperbolic tangent, $\rho(z)=\rho_0-\delta\rho\tanh[(z-z_0)/d]$, and found a nonzero nonlinear (quadratic) coefficient. Solitary waves were generated as a result of the collapse of a mixed region in the pycnocline, which was caused by a rotary paddle mixer.

A typical photograph of the solitary wave shape and a temporal record of a wave form as measured by a hot-film probe are depicted in Fig. 5. Qualitatively, the solitary waves in this experiment were similar to those observed by Davis and Acrivos[16]—they have a form of antisymmetric second-mode perturbation in the intermediate layer. The characteristic scales of these solitary waves were about 3.5 cm, so that the JKKD model should be applicable in this case instead. Nevertheless, the authors claims that the KdV theory was valid when compared with the experiment. They concluded "the agreement between the experiment and the theory is found to be excellent." The main characteristics tested were as follows:

(a) The wave profile, which was in unexpectedly good agreement with the KdV soliton shape as described by Eq. (6) in spite of a breach in the long-wave approximation; and
(b) The nonlinear correction to the wave speed normalized by linear velocity, $(V-c)/c$, versus the amplitude of the normalized particle velocity, $u_{\max}/c$, which was in satisfactory agreement with Eq. (7), even for relatively large values up to 0.7 of the former ratio.

Even better agreement between experimental data and theory was obtained by Kao, Pan, and Renouard in 1985,[18] who conducted their experiment within the framework of validity of the KdV theory. The same water tank as discussed above was filled with layers of saltwater of thickness h_2 at the bottom and with freshwater of thickness h_1 at the top. The resultant density profile was measured very carefully, and could be fitted by a hyperbolic tangent profile as in the above case, with an interface thickness $d=0.3-1.3$ cm. In these experiments, a wide range of variations of the mid-pycnocline level was used: from 0.95 to 7.6 cm below the free surface, so that the ratio of total fluid depth H to the upper layer depth h_1 varied from 4.5 to 36.

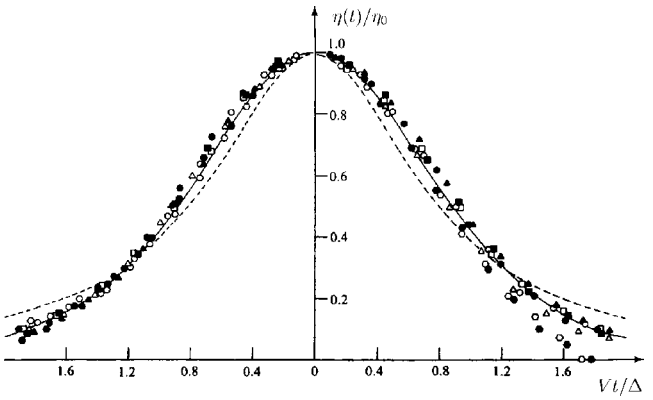

FIG. 6. Comparison of several sets of experimental data with KdV (solid line) and BO (dashed line) solitons for a shallow-water configuration. Filled circles—$h_1/H=\frac{1}{18}$; open circles—$h_1/H=\frac{1}{21}$; filled triangles—$h_1/H=\frac{1}{14}$; open triangles, filled and open squares—$h_1/H=\frac{1}{7}$ with different soliton amplitudes; filled and open hexagons—$h_1/H=\frac{3}{14}$ with different soliton amplitudes. From Ref. 18.

The first-mode solitary waves observed in that experiment had negative polarity, because the thickness of the upper layer was always less than of the lower one. The first eigenmode and the eigenvalue c for the corresponding Sturm–Louiville problem were calculated numerically, and then the coefficients α and β of the KdV equation were evaluated. Then, experimental data were compared with the KdV theory, giving excellent agreement, particularly for smaller values of h_1/H. A sample plot of the solitary wave profiles for several values of the h_1/H ratio is depicted in Fig. 6, with the theoretical shapes of the KdV (solid line) and BO (dashed line) solitons displayed.

The other important characteristics of solitary waves also demonstrate very good correlation with the KdV theory. In Fig. 7 one can see the normalized nonlinear correction to the wave speed $\bar{V}_{\rm nl}\equiv(V-c)/(0.5\alpha H)$ versus the normalized amplitude. The noticeable deviations from the KdV theory in this picture are seen for strongly nonlinear solitary waves

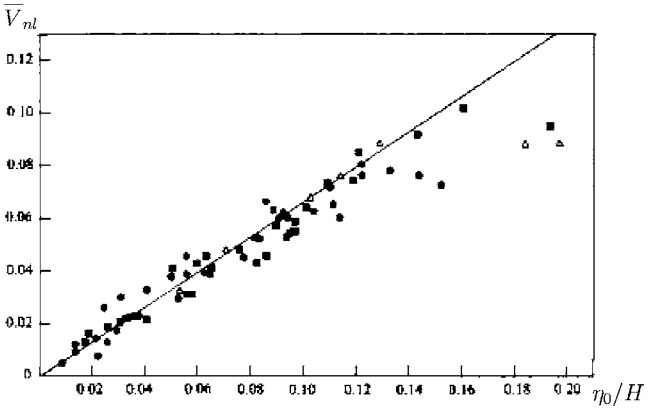

FIG. 7. Normalized phase speed, $(V-c)/(0.5\alpha H)$, for solitary waves in a shallow-water tank as a function of the normalized wave amplitude, η_0/H. Filled circles—$h_1/H=\frac{1}{14}$; filled squares—$h_1/H=\frac{1}{7}$; open triangles—$h_1/H=\frac{3}{14}$; the solid line is the KdV theory. From Ref. 18.

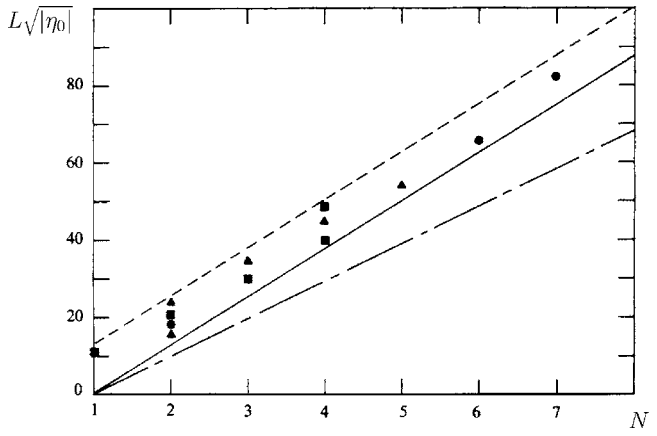

FIG. 8. Number of solitons formed from a pulse-type initial perturbation (on the horizontal axis) versus the product $L\sqrt{|\eta_0|} \sim \sqrt{\mathrm{Ur}}$. Solid and dashed lines are theoretical predictions which follow from different approximations of a smooth density profile; the dashed-dotted line is the lower boundary from the two-layer theory. Symbols are experimental data. From Ref. 18.

that are beyond the range of validity of the KdV theory. It was also shown that under these experimental conditions, the use of a two-layer model is less satisfactory than that of a continuous model with a hyperbolic tangent approximation; e.g., the linear velocity c for the former model is about 10% greater than for the latter (which is closer to the experimental data). Note that the same feature was pointed out by Gan and Ingram[19] in their interpretation of field observations of solitons in Manitounuk Sound (southern Hudson Bay). They made a comparison of the measured characteristics of the solitary waves with both the theoretical predictions within the framework of the usual first-order KdV model based on continuous stratification and with the second-order KdV model (with high-order nonlinear and dispersive terms) for a two-layer fluid. Their conclusion is "the former model may be even closer to the observed values" than the latter one.

The number of solitons arising from a long pulse-type initial perturbation also corresponds well to the theoretical prediction. As is known (see, e.g., Refs. 2 and 20), the number of solitons is determined by the Ursell parameter, $\mathrm{Ur} = \alpha \eta_0 L^2/\beta$, where η_0 is the amplitude of the initial perturbation and L is its characteristic scale. (This parameter is known in nonlinear wave theory as the similarity parameter of the KdV equation.[20] We use throughout the term "Ursell parameter" from the surface-wave terminology and apply it to the topic of general water waves.) In particular, for the initial perturbation of a sech^2 shape and large Ur, the number of solitons is $N \approx \sqrt{\mathrm{Ur}/6}$. The number of solitons generated from the initial perturbation is shown in Fig. 8 versus the product $L\sqrt{|\eta_0|}$, which is proportional to $\sqrt{\mathrm{Ur}}$ and characterizes the nonlinearity of the initial perturbation. The authors note that the two-layer approximation leads to the overestimation of the number of solitons.

In the experimental papers[21–23] some noticeable discrepancies with theoretical models were found. In these experiments a two-layer fluid with a thin lower layer was typically used (although some experiments[23] used a thick lower layer as well). The use of the two-layer model for data interpretation was quite reasonable in experiments with immiscible liquids:[21,23] water ($\rho_1 = 1$ g/cm^3) and freon TF ($\rho_2 = 1.58$ g/cm^3) in Ref. 21 so that $\rho_1/\rho_2 \approx 0.63$, and kerosene ($\rho_1 = 0.8$ g/cm^3) or khladon-113 ($\rho_1 = 0.67$ g/cm^3) and water ($\rho_2 = 1$ g/cm^3) in Ref. 23 with density ratios $\rho_1/\rho_2 = 0.8$ or 0.63. On the other hand, Segur and Hammack[22] utilized salt-water in the lower layer and freshwater in the upper ($\delta\rho/\rho_2 = 0.048$) with an interface thickness, d, of about 1–2 cm. As was mentioned above, the finite thickness of the pycnocline may lead to significant discrepancies between experimental data and predictions based on the two-layer model. Such discrepancies have actually been discovered and will be discussed below.

The dimensions of the tank used by Koop and Butler[21] were 600 cm $\times$ 45 cm $\times$ 60 cm. Two sets of experiments were carried out: with depth ratios of $h_1/h_2 \simeq 5.1$ and 35. In the experiments by Segur and Hammack,[22] the water tank was fairly long, 3000 cm $\times$ 60 cm $\times$ 39.4 cm, with a thin lower layer, $h_2 = 5$ cm and constant depth ratio, $h_1/h_2 \simeq 9$. Bukreev and Gavrilov[23] used a tank of 220 cm $\times$ 15 cm $\times$ 15 cm, with different depth ratios of liquid layers varying in the range of 0.357–3.5.

Qualitatively, the evolution of an initial pulse occurred in a similar way in all experiments described above, both for the first and second modes, thereby demonstrating that solitary waves can emerge from a wide class of initial perturbations having, in these cases, a positive polarity that is appropriate for a thinner lower layer, in accord with the theory. As expected, for a negative polarity of the initial perturbation, no solitons were observed, but dispersive wave trains emerged instead.

Measurements of soliton profiles in all three papers mentioned above,[21–23] have shown reasonably good agreement with a theoretical prediction within the KdV model when it is applicable. Meanwhile, Bukreev and Gavrilov[23] found a noticeable deviation from the KdV soliton shape when the amplitude of the solitary wave was relatively large, $\eta_0/h_2 = 0.2$, whereas for small amplitudes, $\eta_0/h_2 = 0.1$, the agreement between theory and experiment was very good. Actually, it was discovered in that paper that soliton broadening occurs when the soliton amplitude increases, although this effect was not studied systematically. The authors compared their data with Keulegan's theory[11] obtained for the "two-directional" Boussinesq equation and found that the frontal part of a measured solitary wave was closer to the KdV soliton (6), whereas the rear part was closer to Keulegan's soliton, Eq. (11). This apparent difference in the KdV and Keulegan's soliton profiles is probably caused by the misprint in Keulegan's paper,[11] which resulted in a $\sqrt{3/2}$ times larger soliton width. The broadening in the rear part of the solitary-wave profile observed in the experiment[23] could be caused by viscous effects. As was shown in Ref. 24, certain types of dissipation, e.g., Reynolds dissipation, can result in the broadening of the rear part of a soliton due to the appearance of a shelf behind the soliton. Note, however, that such soliton broadening was not detected by Koop and Butler[21] for a shallow-water configuration ($h_1 = 6.948$ cm, $h_2 = 1.366$ cm, $h_1/h_2 \approx 5.1$) when the soliton amplitude varied in the fairly large range $0.04 < \eta_0/h_2 < 0.7$. The authors[21] concluded "examination of the results reveals that the agreement between

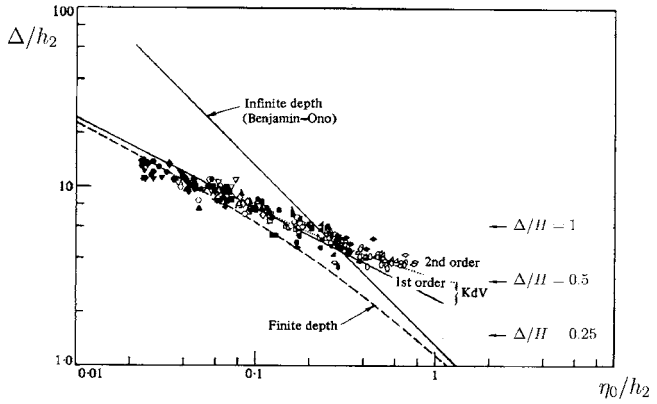

FIG. 9. Dependency of normalized soliton characteristic wavelength Δ/h_2 on normalized amplitude η_0/h_2 as predicted by different theories and measured in the shallow-water experiment. The solid line denoted "first order" corresponds to the usual KDV equation (3); the dotted line denoted "second order" corresponds to the generalized KDV equation with second-order nonlinear and dispersive corrections; the dashed line denoted "finite depth" corresponds to the JKKD equation (26); and another solid line denoted "infinite depth" corresponds to the BO equation (26). From Ref. 21.

the shallow-water data and the 'sech^2' profile predicted by the KdV theory is quite good."

Solitary wave profiles were also measured in Ref. 21 for a deep-water configuration ($h_1=47.87$ cm, $h_2=1.366$ cm, $h_1/h_2\approx 35.0$). Experimental data for solitary waves of different amplitudes, $0.06<\eta_0/h_2<0.6$, showed a noticeable deviation from the KdV-soliton profile grouping around a slightly wider JKKD-soliton profile with the relative amplitude $\eta_0/h_2=0.06$ (the JKKD-soliton shape depends on the amplitude, even in normalized variables). Note that the JKKD soliton with $\eta_0/h_2=0.6$ is practically indistinguishable from the BO soliton, which is the widest among the three KdV, JKKD, and BO solitons. Therefore, one may expect that solitary-wave profiles in the indicated range of amplitudes should lie in the gap between the JKKD soliton with $\eta_0/h_2=0.06$ and the BO soliton, whereas in reality they are centered around the JKKD profile with $\eta_0/h_2=0.06$. The authors concluded that this comparison "does not yield a conclusive result."

Other discrepancies in the soliton parameters were also discovered. Thus, soliton speeds measured by Bukreev and Gavrilov[23] were systematically less than those which the KdV theory[9] predicts for soliton amplitudes in the range of $0.04<\eta_0/h_2<0.6$. Meanwhile, the experimental data were in good agreement with Keulegan's theory[11] rather than with the KdV theory. Different configurations were tested with h_1/h_2 varying within a range 0.36–3.3, so that both positive and negative polarity solitary waves were generated. The results were similar for both types of solitary waves.

Segur and Hammack[22] also registered solitary wave speeds smaller than those predicted by the KdV theory for a two-layer model, and sometimes even less than the speed of long linear waves, c. The reason for this is apparently the finite thickness of the pycnocline, d, which was approximately the same as in Ref. 18.

Another difficulty is in the interpretation of the amplitude-length relationship. In Fig. 9 taken from Ref. 21, such a relationship is depicted for the shallow-water configuration when the depth ratio was $h_1/h_2\approx 5.1$. In this figure one can see rather good agreement between the KdV theory and experimental data up to relatively high soliton amplitudes, $\eta_0/h_2\approx 0.4$. This is somewhat unexpected because the KdV model is formally valid only for small-amplitude perturbations when $\eta_0/h_{1,2}\ll 1$ and for large wavelengths, $\Delta \gg h_{1,2}$, whereas in the experimental situation the soliton wavelength was only several times greater than the thickest layer depth, $\Delta/h_1\approx 1-3$. Hence, one can conclude that, in this case, the approximate KdV theory is robust, even beyond its formal range of validity.

Koop and Butler derived a "second-order KdV equation" for internal waves with second-order nonlinear and dispersion corrections (a similar equation was derived earlier by Lee and Beardsley in 1974;[25] then by Gear and Grimshaw in 1983[26] and by many others). Based on this equation, they obtained a correction to the soliton profile and improved the relationship between soliton amplitude and the wavelength. In Fig. 9 this relationship is shown by the dotted line. As one can see, the improved theory agrees much better with the experimental data up to fairly high amplitudes, $\eta_0/h_2\approx 0.8$.

Meanwhile, in the small-amplitude range, the KdV theory (as well as the improved KdV model that asymptotically coincides with the usual KdV theory at small amplitudes) predicts slightly greater values of soliton wavelengths than what follows from the experiment (see Fig. 9). The authors attribute this to the influence of viscosity in the laminar boundary layers (see a further discussion in the subsequent section).

It is not surprising that the BO model is not well correlated with the experimental data, where both layers are comparable with the characteristic wave scales. In Fig. 9, the BO dependency is indicated only for an illustration. However, the JKKD model is also astonishingly poorly correlated with these data (see the dashed line in Fig. 9 labeled "Finite depth"). Later, Segur and Hammack[22] showed that the improved JKKD model with second-order nonlinear and dispersive corrections correlates with the experimental data by Koop and Butler[21] quite well, similarly to the second-order KdV equation. From a practical point of view, there is no reason to use the fairly complex second-order JKKD model when the second-order KdV equation gives the same results. And an even much simpler KdV equation can satisfactorily approximate the experimental data.

In another experimental realization, where the depth ratio was increased to $h_1/h_2\approx 35$, none of the theories gave a reasonable correlation with the experimental data, even though the JKKD or maybe even the BO models should have worked in this range (Fig. 10). The second-order JKKD model does not help; in this case it gives almost the same dependency between the soliton wavelength and the amplitude as the usual JKKD model (the details can be found in Ref. 22). It is interesting to note that even in this case that is explicitly beyond the applicability limits of the KdV model, the slope of the best-fit line of experimental points in Fig. 10 is close to the slope predicted by the KdV model, although the experimental points are shifted downward with respect to the KdV line.

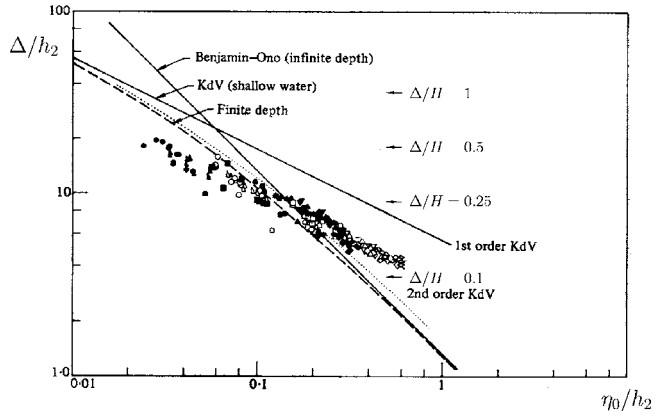

FIG. 10. The same as in Fig. 9, but for the experiment with a deeper upper layer and shallow lower layer. From Ref. 21.

The main cause of all these disagreements is apparently the deviation of experimental conditions from the theoretical requirements, implying that the wave amplitude must be small enough, whereas wavelengths must be long compared to layer thicknesses or long with respect to one layer and small with respect to another one for the BO model. The pycnocline thickness must be small in comparison with the solitary wavelength if the two-layer model is used for comparison with a theory. The influence of viscosity, which is always presents in real experiments, can also explain some discrepancies between the inviscid theory and experimental data.

IV. NONINTEGRABLE MODELS OF INTERNAL WAVES

A. Dissipation modified KdV equation

For conditions generally existing in both the laboratory and in nature, the simple models considered above are rarely applicable without taking into account a number of perturbing factors, such as the dissipation of various origins, wavefront curvature, horizontal inhomogeneities, depth variation, and the like. However, these factors are often locally weak enough so that their effects become significant only at large distances compared to a wavelength. Under these conditions, perturbation theory is generally applicable. Such an approach results in the appearance of small additive terms in the model equation, each responsible for a specific perturbing factor. As an example, for waves much longer than the total depth of the controlling layer, the perturbations mentioned previously may be taken into account within the framework of a generalized "time-like KdV" (TKdV) equation (in the context of oceanic internal waves see, for example, Ref. 27):

$$\frac{\partial \eta}{\partial x}+\frac{1}{c}\frac{\partial \eta}{\partial t}-\frac{\alpha}{c^2}\eta\frac{\partial \eta}{\partial t}-\frac{\beta}{c^4}\frac{\partial^3 \eta}{\partial t^3}=-\hat{R}(\eta). \tag{29}$$

[Such a version of the KdV equation with transposed temporal and spatial variables is relevant to waves excited at a fixed spatial point. It has been used at least since the 1970s (see, e.g., Ref. 28). The name "time-like KdV" was apparently introduced by Osborne.[29] One can also encounter the term "KdV equation in the signaling coordinates."[30]]

The term $\hat{R}(\eta)$ on the right-hand side has a different structure depending on the effect taken into account (see, e.g., Refs. 4 and 6). Here we consider only the dissipation caused by viscous effects in laminar boundary layers occurring in the laboratory tanks. This leads to the inclusion of a fairly complex integral term into Eq. (29)[4,21,31–35]

$$\hat{R}(\eta)=\delta_1\int_{-\infty}^{+\infty}\frac{1-\mathrm{sgn}(t-t')}{\sqrt{|t-t'|}}\frac{\partial \eta(t',x)}{\partial t'}dt'. \tag{30}$$

(Other types of dissipation and their influence on soliton decay in shallow water are analyzed in Ref. 30.)

In general, the dissipation coefficient δ_1 depends on many parameters such as depth, density, and viscosity of fluid layers.[10] In the Boussinesq approximation with the additional assumption that kinematic viscosities of layers are also equal, $\nu_1=\nu_2\equiv\nu_m$, this coefficient may be presented in the form[35]

$$\delta_1=\frac{1}{4c}\frac{\sqrt{\nu_m/\pi}}{h_1+h_2}\left(b+\frac{(1+b)^2}{2b}+2\frac{h_2}{W}(1+b)\right), \tag{31}$$

where $b=h_1/h_2$ and W is the width of the tank. [A misprint in the numerator of formula (A6) of Ref. 36 should be mentioned, it must be a product of depths rather than their difference.] The applicability of this dissipation model requires the boundary-layer thickness to be much less than the total water depth.

The equation (29) with the nonzero right-hand side is nonintegrable; however, a perturbation theory can be used for its solution if the term $\hat{R}(\eta)$ is small enough (see, e.g.,4 and 36). In the simplest case, the concept of energy balance can be used for the description of slow variation of the soliton amplitude η_0 over large distances (much larger than the characteristic soliton width). The corresponding first-order ordinary differential equations are usually integrable, and soliton amplitude variation in space can be readily obtained. This approach is equivalent to the application of one of the versions of the perturbation theories mentioned above, in the lowest order of approximation. When the variation of soliton amplitude with distance is found, the variations of other parameters, time duration, spatial width, and velocity of the soliton can be obtained via the local relations, Eq. (7).

Omitting the details, here we present the resulting variation of soliton amplitude in space for the particular case of small dissipation in the laminar boundary layer:[10]

$$\eta_0(x)=\frac{\eta_0(0)}{(1+x/X_{\mathrm{ch}})^4}\underset{x\to\infty}{\to}\left(\frac{12h_2(1+b)}{b+\frac{(1+b)^2}{2b}+2\frac{h_2}{W}(1+b)}\right)^4\frac{c^2h_1^2h_2}{|b-1|\nu_m^2x^4}, \tag{32}$$

$$X_{\mathrm{ch}}=\frac{12h_2(1+b)}{b+\frac{(1+b)^2}{2b}+2\frac{h_2}{W}(1+b)}\sqrt[4]{\frac{c^2h_1^2h_2}{|b-1|\nu_m^2\eta_0(0)}}. \tag{33}$$

(As pointed out in Ref. 10, the expression for the decay coefficient derived in Ref. 21 is actually incorrect.)

Here $\eta_0(0)$ is the initial soliton amplitude at the point $x=0$, X_{ch} is the characteristic length of soliton decay [note that it depends on the initial soliton amplitude $\eta_0(0)$], $a=\rho_1/\rho_2$, $b=h_1/h_2$, and W is the tank width.

As one can see, in contrast to linear perturbations, soliton decay is nonexponential and at large distances, $x \gg X_{ch}$, the soliton amplitude ceases to depend on its initial value at all $\eta_0(x) \sim x^{-4}$.

B. Nonlinear waves in rotating fluids

1. Plane waves in a rotating fluid

To study mesoscale oceanic processes having spatial scales of a few or more kilometers and time durations of an hour or more, one needs to take into account rotation effects caused in nature by the Earth's rotation. In this case there arise some radically new features in the behavior of nonlinear waves caused by rotation. A detailed mathematical analysis of possible model equations that followed from a primitive set of hydrodynamic equations at different rotation rates was done by Grimshaw[37] and later reproduced by Renouard and Germain.[38] These authors considered the case of relatively small rotation when the parabolicity of the free water surface or interface between two liquid layers can be neglected and both these surfaces can be treated as a quasiplane. The effect of rotation can be formally characterized by the dimensionless Coriolis parameter $F_C=f/\sqrt{(1-a)g/(h_1+h_2)}$, where $f=2\Omega$ with Ω being the frequency of fluid rotation and $a=\rho_1/\rho_2$ as previously.

As was shown for the first time by Ostrovsky[5] (see also Refs. 37–40 and references therein), weakly nonlinear waves in a shallow fluid can be described by the rotation modified Korteweg–de Vries (rKdV) equation:

$$\frac{\partial}{\partial x}\left(\frac{\partial \eta}{\partial t}+c\frac{\partial \eta}{\partial x}+\alpha\eta\frac{\partial \eta}{\partial x}+\beta\frac{\partial^3 \eta}{\partial x^3}\right)=\frac{f^2}{2c}\eta. \tag{34}$$

[Sometimes it is referred as the Ostrovsky equation (see, e.g., Refs. 4, 38, 41, and 42).]

Its derivation presumes that the nonlinearity (the term proportional to α) and both Boussinesq and Coriolis dispersions (the terms proportional to β and f^2, respectively) are small in comparison with the first two linear terms. However, the small terms cited can differ between each other in their order of smallness. The analysis performed in Refs. 37 and 38, was made for the case where the nonlinearity and Boussinesq dispersion are of the same order of smallness, say, $\sim\varepsilon^2$, where $\varepsilon \ll 1$ is a small parameter. If the Coriolis term is of the order of ε^q with $q \geqslant 4$, then the rotation effect is completely negligible so that the right-hand side of Eq. (34) can be omitted, and it reduces after integration to the usual KdV equation. As noted in Refs. 37 and 38, in this case of "extremely weak rotation" ($q=4$), the only new effect is an appearance of the transverse fluid velocity component that is, however, of the higher order of smallness with respect to the longitudinal component.

In the case of "very weak rotation" ($q=3$) the right-hand side of Eq. (34) can be treated as a small perturbation of the KdV equation. In this case one can develop an asymptotic approach to the evolution of nonlinear waves (and KdV solitons in particular) under the action of perturbation. An interesting new result is that the KdV soliton undergoes a "terminal decay," i.e., it completely annihilates (more exactly, transforms into radiation) in a finite time.[40,43] The soliton amplitude varies with the distance in accordance with the formula

$$\eta_0(x)=\eta_0(0)\left(1+\frac{f^2}{2c}\sqrt{\frac{12\beta}{\alpha\eta_0(0)}}(x_0-x)\right)^2, \tag{35}$$

where $\eta_0(0)$ is the soliton amplitude at some initial point $x=x_0$.

At some stage when the radiation amplitude becomes comparable with the soliton amplitude, the asymptotic theory ceases to work. However, numerical calculations[43,44] show that when the initial soliton disappears, a new pulse whose shape is close to a KdV soliton forms from the leading edge of radiation so that some sort of recurrence phenomenon takes place.

When the rotation term in Eq. (34) is of the same order as the nonlinear and dispersive terms, i.e., $q=2$ ("weak rotation" case according to Ref. 38), exact analytical solutions of Eq. (34) are unknown, even for stationary waves. However, many of their features have been investigated by now. In spite of that, Eq. (34) is apparently nonintegrable, and it possesses some integrals of motion, e.g., integrals of mass and energy conservation. Besides, a number of integral invariants exist in the form of constraints that dictate some restrictions on the class of admissible initial perturbations. In particular, as follows from Eq. (34), the total "mass" of perturbation,

$$M \equiv \int \eta(x,t)dx, \tag{36}$$

must be zero if the perturbation is smooth enough so that the integral is determined and finite. For periodic perturbations, the integration in Eq. (36) is taken over the wave period, whereas for solitary waves the integration is taken over the entire axis x. Note that for the previously considered integrable equations such as the KdV, mKdV, eKdV, BO, and JKKD equations, this integral is an arbitrary constant (not necessarily zero) to be determined by initial conditions.

A relatively simple analysis of stationary solutions of Eq. (34) can be performed if the Boussinesq dispersion (the term with β) is neglected, which is possible for sufficiently long waves. A corresponding reduced version of Eq. (34) with $\beta=0$ was analyzed by Ostrovsky[5] for the first time. A similar equation with $\beta=0$ was also obtained later for different types of waves (see, e.g., reviews[39,40] as well as a paper[45] for references). A detailed analysis of stationary solutions is presented in Refs. 46 and 95. From the point of view of a practical application in fluid dynamics the most interesting stationary solutions to that reduced equation represent a family of periodic waves whose shape varies with amplitude from sinusoidal to parabolic.

An important peculiarity of equations, Eq. (34), is that for the Boussinesq-type dispersion of gravity waves [when the coefficient β in Eq. (34) is positive], solitary waves in the form of stationary localized pulses cannot exist at all.[42,47,48]

In spite of this rigorously proven result, an approximate stationary soliton solution to the rKdV equation with the zero total mass was constructed in Ref. 38 (they referred to it as the "Ostrovsky wave"). Apparently the solitary solution obtained in that paper in the form of a series relates to the case of $\beta<0$ (in our notations). In this case, the "antisoliton theorem" mentioned above is not valid, and solitary solutions can exist. Indeed, they were found numerically in Refs. 48 and 49.

In addition to stationary solutions, some nonsteady solutions for the rKdV equation have also been studied, mostly numerically.[39,44] It was confirmed that the initial KdV soliton decays in a finite time, as predicted by the asymptotic theory.[40,43] [More precisely, a periodic sequence of solitons on a small negative background was considered to satisfy the zero-mass condition (36).] During this process of terminal decay, the soliton background tends toward the parabolic shape mentioned above.

Another interesting example of a nonstationary wave propagation within the framework of the rKdV equation shows that despite the antisoliton theorem,[42,47,48] which prohibits the existence of stationary solitary waves, the nonstationary solitary waves can coexist with smooth periodic perturbations of small amplitude and large wavelength. The solitary wave shape is very close to a KdV soliton, and its amplitude and other related parameters vary adiabatically in time and space due to the interaction with a large-scale wave. During some special conditions when the KdV soliton is matched with a periodic sequence of parabolic arcs, a steady-state wave forms.[50]

In the case of "strong rotation" ($q=1$) (but still weak enough to neglect the parabolic curvature of internal and external surfaces of liquid layers), Eq. (34) becomes linear with negligible nonlinearity and Boussinesq dispersion. Wave dynamics in this case can be studied by traditional linear methods based on Fourier analysis, and their asymptotics can be calculated by means of the stationary phase method (see, e.g., Ref. 2). There are also more general versions of shallow-water models (rotation-modified Boussinesq equations) that account for weakly nonlinear "two-directional waves," i.e., waves propagating in opposite directions.[41,51] Strongly nonlinear interfacial waves in a two-layer rotating fluid but without Boussinesq dispersion were studied theoretically by Plougonven and Zeitlin.[52] In these papers neither nonlinearity nor rotation is presumed small.

The main conclusion drawn from this section is that the rotation acts destructively on solitons of gravitational waves. Stationary solitons do not exist at all when $\beta>0$, both within the rKdV equation and more general two-directional equations. A KdV soliton taken as an initial perturbation for the rKdV equation with a small rotation effect undergoes terminal decay and disappears in a finite time. Nevertheless, nonstationary solitary waves, very close to KdV solitons, can exist on a long periodic perturbation.

2. Rotation-modified cylindrical KdV equation

In nature and in some laboratory experiments, waves excited by localized sources eventually become circular in the horizontal plane. At this stage the amplitude of the perturbation decreases due to cylindrical divergence. The evolution of the parameters of a nonlinear, cylindrically divergent wave, especially in the presence of rotation, can occur in a complicated way. Laboratory experiments can provide valuable data for understanding different regimes of cylindrical wave propagation and decay.

In application to nonlinear waves in nonrotating shallow water, the problem of cylindrical spreading was intensively studied in the 1970s; analogous problems were also considered in plasma physics and in other areas of physics. A review of these results can be found in Refs. 53 and 54. A brief summary of the results are as follows.

Long, weakly nonlinear waves with circular fronts in rotating fluids can be described by the rotation-modified cylindrical Korteweg–de Vries equation. In the signalling coordinates (when temporal and spatial coordinates are interreplaced) the equation has the form:[55]

$$\frac{\partial}{\partial t}\left(\frac{\partial \eta}{\partial r}+\frac{1}{c}\frac{\partial \eta}{\partial t}-\frac{\alpha\eta}{c^2}\frac{\partial \eta}{\partial t}-\frac{\beta}{c^4}\frac{\partial^3 \eta}{\partial t^3}+\frac{\eta}{2r}\right)=\frac{f^2}{2c}\eta. \tag{37}$$

First consider its particular version for the case of nonrotating fluid, $f=0$. The corresponding equation is known as the cKdV equation.[28,56,57]

Amplitude variation versus radial coordinate r for a pulse-type perturbation within the framework of this equation depends on the relationship between the terms responsible for the effects of nonlinearity, dispersion, and geometrical spreading.

For linear dispersionless perturbations, the well-known law $\eta_0 \sim r^{-1/2}$ readily follows for the wave amplitude. If the characteristic scale of the initial pulse is comparable with the water depth, the dispersion can no longer be neglected, and the pulse spreads in space and time, eventually transformed into a wave train. The wave train behind its front decreases due to both the dispersion effect and the geometrical spreading, resulting in the law $\eta_0 \sim r^{-1}$, whereas its leading edge decreases as $\eta_0 \sim r^{-5/6}$.[55]

For finite-amplitude perturbations, when nonlinearity and dispersion are balanced and cylindrical spreading is weak enough, an approximate solution to Eq. (37) in the form of a perturbed KdV soliton with gradually changing amplitude, $\eta_0 \sim r^{-2/3}$ and wavelength $\Delta \sim r^{1/3}$, can be derived (apparently, it was derived initially by Iordansky[56]). Behind the soliton an oscillatory tail forms in the process of propagation. This law of soliton decay can be readily obtained by means of the perturbation method or just from the soliton energy conservation. Numerical results confirm this law very well (see line 1 and corresponding numerical data in Fig. 11, later).

The same dependencies of wave parameters on distance (at least in a certain spatial domain, far from the center) follow from the exact solution of the cKdV equation. As shown by many authors (see, e.g., Refs. 58 and 59), this equation belongs to the class of completely integrable systems. In particular, two independent analytical solutions (nonlinear modes) were constructed for this equation. They have a different structure but evolve similarly in space. The first mode, described by the first kind of Airy function, $\mathrm{Ai}(\xi)$,[58] is not well localized; it represents an oscillatory non-

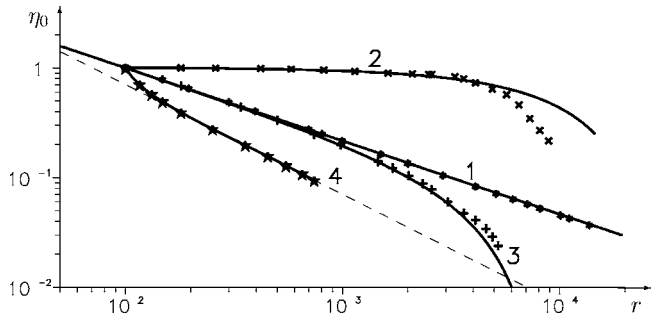

FIG. 11. A comparison of solitary wave decay within the framework of a rotation-modified cKdV equation with and without rotation, as predicted by approximate theories and calculated numerically. For details see text. (From Ref. 55.)

linear wave train. The second mode, described by the second kind of Airy function, $\mathrm{Bi}(\xi)$,[59] represents a pulse-type perturbation with a small oscillatory tail in the rear part. This mode looks similar to a cylindrically diverging solitary wave observed in experiments and numerical calculations (see, e.g., Refs. 53 and 54 and references therein).

For waves affected by fluid rotation, both the model equation and the laws of wave evolution are modified. The resultant rotation-modified cKdV equation, Eq. (37), becomes nonintegrable.

The influence of rotation on the amplitude variation of pulse-type internal waves in shallow water was theoretically studied in Ref. 55. The results can be summarized as follows.

The amplitude variation with distance for a perturbed KdV soliton was obtained with the use of an energy balance equation:

$$\eta_0(r) = r^2\left[\left(\frac{\eta_0(0)^{1/2}}{r_0} + \frac{3f^2}{8c}\sqrt{\frac{12\beta}{\alpha}}\right)\left(\frac{r}{r_0}\right)^{-4/3} - \frac{3f^2}{8c}\sqrt{\frac{12\beta}{\alpha}}\right]^2. \tag{38}$$

In one limiting case, when the rotation is absent, the law of soliton decay due to cylindrical spreading, $\eta_0 \sim r^{-2/3}$, readily follows from this equation. In another limiting case, when there is no cylindrical divergency (the plane soliton propagating in a rotating fluid), the expression (35) for the "terminal decay" of the KdV soliton can be recovered.

Figure 11 shows a comparison of theoretical and numerical results obtained within the framework of the rotation-modified cKdV, Eq. (37), for the same initial perturbation having the form of a KdV soliton, Eq. (6).

For a cylindrically diverging soliton in the nonrotating case, numerical and theoretical results are in excellent agreement (see line 1 and asterisks in Fig. 11). It was found that the soliton gradually changes its shape and acquires a very small negative tail due to the influence of radial spreading. However, these variations are so small that they are almost invisible in a scale of amplitudes even at long distances. The relationship between amplitude and characteristic duration of a solitary wave is in good agreement with the formula (7) for the KdV soliton, $T \sim \eta_0^{-1/2} \sim r^{1/3}$.

The attenuation of a plane soliton due to weak rotation as predicted by Eq. (35) is presented by line 2 and crosses in Fig. 11. Some discrepancy between theory and numerical data at large distances was caused by the influence of radiated waves. (The calculations were performed with periodic boundary conditions; therefore, the radiated waves eventually began to interact with the main pulse. The increase of the period decreased the discrepancy.) In comparison with the nonrotating case, the radiated tail behind the pulse was very intensive and increased with the distance.

The simultaneous action of weak rotation and cylindrical divergence on a KdV soliton is illustrated by line 3 and pluses in Fig. 11. As one can see, the results obtained agree with the theory, Eq. (38), even better than in the plane case. This can be explained by a more compact tail formed behind the main pulse. Therefore, its effect on the solitary wave manifests itself later in the periodic system.

The result of evolution of the initial KdV soliton in the linear system is depicted in Fig. 11 by curve 4. The synergetic action of rotation, Boussinesq and Coriolis dispersions lead to amplitude decay as $\eta_0 \sim r^{-1}$, in accordance with the theoretical prediction.

C. Strongly nonlinear models

In previous sections, both nonlinearity and dispersion were considered small so that, e.g., in a two-layer fluid, the displacement of the pycnocline is significantly smaller than its equilibrium depth (or, for a pycnocline close to the bottom, than its height over the bottom). In oceanography, along with a number of observations for which the weakly nonlinear models provide a good approximation, there is also a growing amount of data for which they are evidently wrong (see examples in the experimental subsection, V C).

To describe strongly nonlinear internal waves, direct numerical simulation for the basic hydrodynamic equations has been used. In particular, many numerical works considered steady waves in a two-layer fluid. In this case the linear Laplace equation can be used for each layer. The first was probably the paper by Amick and Turner[60] (see also Ref. 61). In addition to a detailed mathematical treatment of the problem, they have shown that there exists a limiting amplitude at which a soliton acquires a flat top and tends to two separated kinks, similar to the case of the eKdV equation, but with different parameters. The amplitude and velocity of such a limiting soliton are

$$\eta_{0\,\mathrm{lim}} = \frac{h_1 - h_2\sqrt{a}}{1+\sqrt{a}}, \quad V_{\mathrm{lim}} = \frac{\sqrt{g(1-a)(h_1+h_2)}}{1+\sqrt{a}}, \tag{39}$$

where $a = \rho_1/\rho_2 < 1$, and positive displacement is the upward one.

Subsequently, a direct numerical analysis of the two-layer case as applied to stationary solitary waves was performed by many authors (see, e.g., Refs. 62 and 63). As an example, Fig. 12 shows calculations of soliton profiles for a two-layer fluid using the parameters chosen by Evans and Ford.[62] More recently, calculations of solitary waves in a layer with smooth stratification were performed. Also, some nonsteady, strongly nonlinear processes were studied by di-

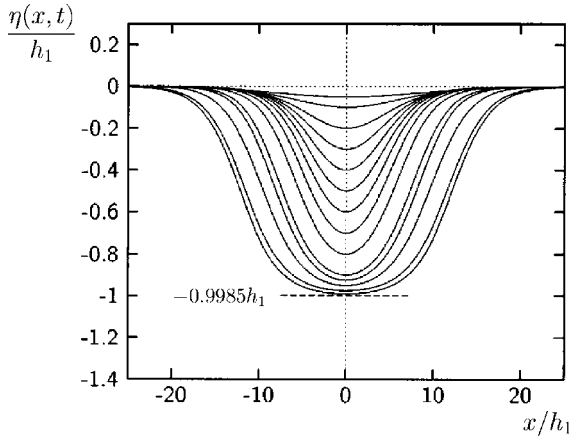

FIG. 12. Soliton profiles, $\eta(x)/h_1$ vs x/h_1, for a two-layer fluid with $h_2/h_1=3$, $\rho_1/\rho_2=0.997$ (the surface is at +1; the bottom at −3 on the vertical axis). The profiles shown correspond to different soliton amplitudes, $-\eta_0/h_1=0.05$; 0.1; 0.2; 0.3; 0.4; 0.5; 0.6; 0.7; 0.8; 0.9; 0.925; 0.95; 0.975; and 0.99. The dashed horizontal line marks the level of the limiting amplitude wave. From Ref. 62.

rect numerical simulation. Vlasenko and Hutter[64,65] modeled the shoaling of long internal waves in coastal areas. These processes include steepening, the formation of soliton groups, and breaking with the generation of turbulence. Lamb[66,67] showed that shoaling of a solitary wave can result in the formation of a trapped core, which was previously observed in the laboratory experiment by Davis and Acrivos.[16] Stastna and Lamb[68] calculated soliton propagation on a background current.

However, direct numerical computations are usually time costly and, also important, it is often difficult to understand the qualitative pattern of the process. Although there are, strictly speaking, no *a priori* small parameters that could be used to simplify the problem, in many cases the soliton length remains much larger than the thickness of one of the layers or of the total depth of the ocean, especially in coastal areas. For these cases, a long-wave approximation can be constructed that uses the corresponding expansion of dispersive terms while keeping the nonlinearity strong. This approach was first suggested by Whitham[69] for surface waves based on the expansion of the Lagrangian.

For internal waves in a two-layer fluid, Miyata was apparently the first who suggested (albeit without a detailed derivation) the long-wave equations for strongly nonlinear, weakly dispersive waves in a two-layer fluid, and analyzed a steady solitary solution of these equations.[70–72] Miyata's equations, together with other weakly nonlinear models, KdV, eKdV, BO, and JKKD, were examined against numerical calculations in (Refs. 71 and 73) (see the experimental subsection, V C). A detailed analysis of the same problem for a two-layer fluid was performed by Choi and Camassa[74] for two layers with arbitrary densities, ρ_1 and $\rho_2>\rho_1$. For shallow water, these equations (essentially the same as those obtained by Miyata), being reduced to the case of a small density jump, $\Delta\rho\ll\rho_{1,2}$, typical of oceanic conditions and most of the laboratory experiments with strong solitons, can be represented in the form

$$\frac{\partial\eta}{\partial t}+\frac{\partial}{\partial x}[(h_1+\eta)u_1]=0, \tag{40}$$

$$u_2=-u_1\frac{h_1+\eta}{h_2-\eta}, \tag{41}$$

$$\begin{aligned}&\frac{\partial}{\partial t}\left(u_1\frac{h_1+h_2}{h_2-\eta}\right)+\frac{1}{2}\frac{\partial}{\partial x}\left(u_1^2\frac{h_2^2-h_1^2-2\eta(h_1+h_2)}{(h_2-\eta)^2}\right)+g'\frac{\partial\eta}{\partial x}\\&=\frac{1}{3(h_1+\eta)}\frac{\partial}{\partial x}\left\{(h_1+\eta)^3\left[\frac{\partial^2u_1}{\partial t\partial x}+u_1\frac{\partial^2u_1}{\partial x^2}-\left(\frac{\partial u_1}{\partial x}\right)^2\right]\right\}\\&\quad-\frac{1}{3(h_2-\eta)}\frac{\partial}{\partial x}\left\{(h_2-\eta)^3\left[\frac{\partial^2u_2}{\partial t\partial x}+u_2\frac{\partial^2u_2}{\partial x^2}-\left(\frac{\partial u_2}{\partial x}\right)^2\right]\right\}.\end{aligned} \tag{42}$$

Here the z axis is directed downward, and $u_{1,2}$ are the horizontal velocities in the layers, each averaged over the layer thickness. After the substitution of u_2 onto the rhs of the last equation, we have two equations for η and u_1. This reduction has been done in Ref. 75, where it was also demonstrated that the set of Eqs. (40)–(42) is a straightforward result of the long-wave expansion of the Lagrangian suggested by Whitham[69] for surface waves.

For a stationary soliton in which all variables depend on one variable $x-Vt$, this system can be reduced to a second-order ordinary differential equation that can be readily analyzed. In particular, as follows from the equation of mass balance, Eq. (40), the current velocities at the soliton crest ($\eta=\eta_0$) and the soliton speed are

$$u_1=\frac{V\eta_0}{h_1+\eta_0},\quad u_2=-\frac{V\eta_0}{h_2-\eta_0}, \tag{43}$$

$$V(\eta_0)=\sqrt{\frac{g'(h_1+\eta_0)(h_2-\eta_0)}{h_1+h_2}}.$$

An evolution equation for a wave propagating in one (e.g., positive) direction (β model) was written in the form[75,76]

$$\frac{\partial\eta}{\partial t}+c(\eta)\frac{\partial\eta}{\partial x}+\frac{\partial}{\partial x}\left(\beta(\eta)\frac{\partial^2\eta}{\partial x^2}\right)=0. \tag{44}$$

Here $\beta(\eta)=[c(\eta)/6](h_1+\eta)(h_2-\eta)$ is the nonlinear dispersion parameter corresponding to the KdV dispersion parameter (see previously) at an instantaneous depth, $h_1+\eta$. The value of $c(\eta)$ is the velocity of a simple wave that is exact if the wave is so long that dispersion can be completely neglected:[77]

$$\begin{aligned}c(\eta)=c(0)\Bigg[1+3\frac{(h_1-h_2)(h_1-h_2-2\eta)}{(h_1+h_2)^2}\\\times\left(\sqrt{\frac{(h_1-\eta)(h_2+\eta)}{h_1h_2}}-\frac{h_2-h_1+2\eta}{h_2-h_1}\right)\Bigg],\end{aligned} \tag{45}$$

where $c(0)\equiv c$ is the velocity of linear perturbations.

It should be emphasized that, unlike in the weakly nonlinear case, the long-wave approximations for surface and internal waves considered above (both two and one direc-

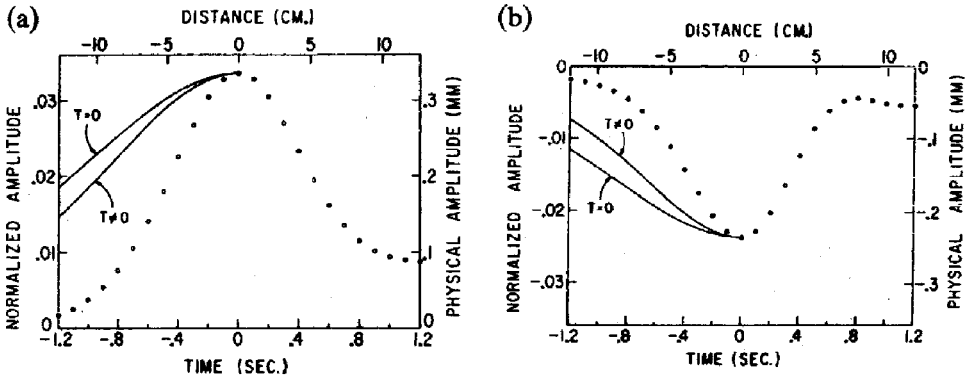

FIG. 13. Comparison of observed solitary wave shapes (open circles) with KdV solitons of the same amplitudes as obtained within the framework of the inviscid KdV equation, both without surface tension (curve labeled by $T=0$) and with surface tensions at the interfaces water Varsol and Varsol air (the curve labeled by $T\neq 0$). (a) shows an elevation wave with $h_2=11.5$ cm, $h_1/h_2=1.25$ $\eta_0/h_2=0.0336$; (b) shows a depression wave with $h_2=11.5$ cm, $h_1/h_2=0.875$ $\eta_0/h_2=-0.0237$. From Ref. 8.

tional) are of a somewhat contradictory nature. Indeed, these equations combine strong nonlinearity and weak dispersion, whereas a soliton exists as a balance between the nonlinearity and dispersion, so that it is *a priori* unclear whether a strong soliton would be long enough to provide sufficiently small dispersion terms and thus secure the applicability of the shallow-water approximation. This makes the verification of these models especially necessary. Such a comparison with the fully nonlinear numerical models has been done, in particular, in Refs. 7 and 74. The corresponding laboratory experiments are described in Sec. V C.

For a very large depth ratio the applicability of the "shallow-water" model is limited because the basin is not always shallow enough for the solitons. For these cases, similar models have been constructed for a thin upper and infinitely deep lower layer both for two-directional and one-directional cases. The corresponding conditions were not created in laboratory experiments, so we do not present the corresponding formulas here (the details can be found in Refs. 7 and 75).

V. LABORATORY EXPERIMENTS EXAMINING NONINTEGRABLE MODELS

A. Soliton damping in laboratory experiments

Evidently, dissipation is present in all experiments. However, in some experiments its effect is relatively small and can be neglected. In others, dissipation was marked as a possible cause of disagreement between theoretical predictions and experimental data, still without a systematic study of its effect. Only in a few papers has the influence of viscosity on internal waves been intentionally studied.

The first such paper was probably that by Walker.[8] He made estimates for a two-layer fluid that shows that due to viscosity one can expect a wave-speed reduction of about 10% in comparison with the inviscid theoretical value, this effect being more pronounced for waves of smaller amplitudes. As was described in Sec. III, two immiscible fluids were used in that experiment, water of density $\rho_2=1$ g/cm^3 in the bottom layer and Varsol I (Humble Oil) of density $\rho_1=0.784$ g/cm^3 in the upper layer. Their viscosities are $\nu_2=0.01$ and $\nu_1=0.015$ cm^2/s, respectively.

Results of wave profile measurements show that the observed solitary waves were "severely narrowed," even with respect to the case when the surface tension effect also leading to wave narrowing is taken into account (Fig. 13). The effect was especially noticeable at small wave amplitudes, whereas at $\eta_0/h_2\geqslant 0.25$ the "narrowing is substantially less." As already mentioned (see Sec. III), the author also found "a small ($<5\%$ in half-width) systematic departure from sech^2 shape for small waves, with those of elevation being steepened in front and broadened in back, and *vice versa* for those of depression." The reader should not be confused with the statement in Sec. III, where we wrote that the author found good agreement between the experimentally measured wave shape and the theoretically predicted sech^2 function in the frontal part of a solitary wave. As one can see from Fig. 13, the deviation of experimental data from theoretical lines is quite significant; nevertheless, the experimental data still can be best fitted by the sech^2 function, but of a different (smaller) time scale. The detected solitary wave profiles were not symmetrical, apparently due to the known effect of viscosity on a soliton (see, e.g., Refs. 24 and 78). Because of that, the comparison of experimental data with KdV theory was made only for the frontal parts of waves (this situation is typical for many experiments of different authors).

Solitary wave velocities were also measured versus wave amplitudes at different depth ratios, then the values extrapolated to $\eta_0\to 0$ were compared with theoretical predictions for long linear waves. It was found that "in general, the speeds are 8% less than those predicted by the inviscid theory and display a rather pronounced decrease" as h_1/h_2 approaches from below to the critical value (where the quadratic nonlinear coefficient α in the KdV equation vanishes).

Another detailed study of the viscosity effect on internal waves was undertaken in Ref. 21. The authors modified Keulegan's results[79] obtained for surface waves to adapt them for internal waves in a two-fluid system. The resultant expression governing solitary-wave amplitude decay is given by Eq. (32) above, with the viscosity coefficients for water $\nu_1=0.01$ cm^2/s and for freon TF $\nu_2=0.0044$ cm^2/s.

The authors carefully studied single-soliton propagation and found that "in actuality, a wave of permanent form is never realized experimentally." In particular, in their tank (see the description in Sec. III), the solitary wave that traveled a distance of 3.5 m and reflected from one of the tank walls was only 30% in amplitude of the incident wave when it returned to the same place.

To quantify the viscous decay of solitary waves, "experiments were performed where multiple reflections off the end walls were monitored in order to increase effectively the dis-

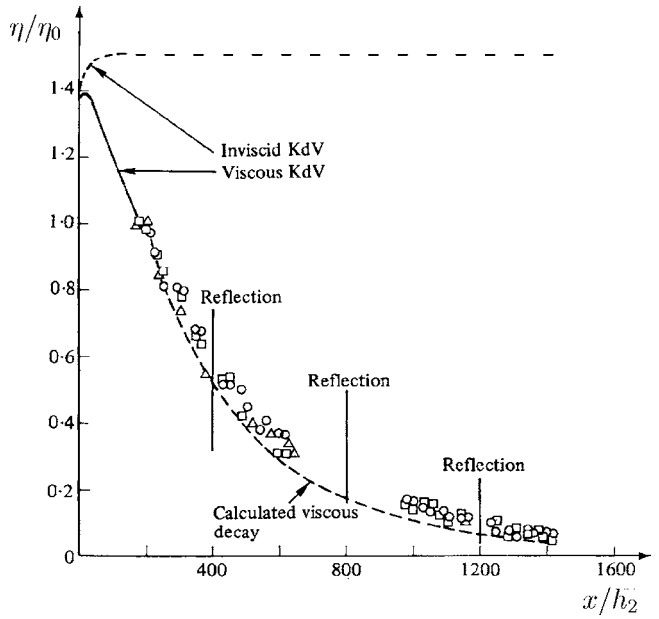

FIG. 14. Comparison of solitary wave decay as calculated numerically (solid line), analytically on the basis of the asymptotic theory resulting in the adiabatic solution, Eq. (32) (dashed line) and experimentally measured. From Ref. 21.

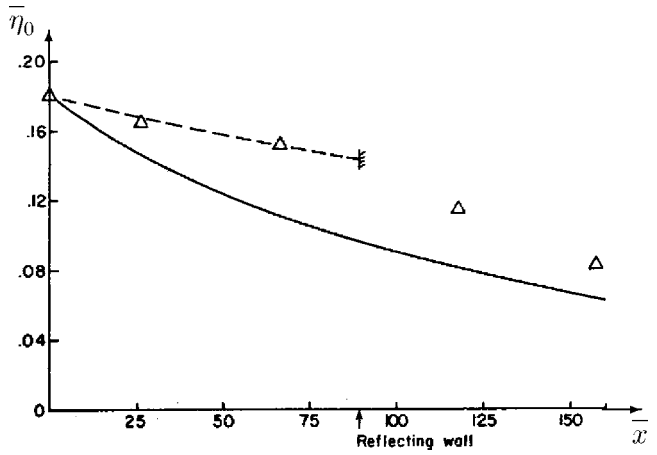

FIG. 15. Comparison of solitary wave decay as calculated on the basis of "improved" (solid line) and "revised" (dashed line) theories for the adiabatic soliton decay described by Eq. (32) and experimental data. From Ref. 10.

tance traveled by given disturbance." The results are presented in Fig. 14. Solitary wave amplitudes are normalized by the incident-wave amplitude measured at some distance from the wavemaker. As already mentioned in Sec. III, the experiment described in Ref. 21 was carried out both for deep- and shallow-water configurations. Circles and boxes in Fig. 14 represent data obtained in the deep-water configuration with initial amplitudes $(\eta_0/h_2)_{2a}=0.305$ and 0.109, respectively. Triangles represent shallow-water data with $(\eta_0/h_2)_{2a}=0.269$. In the same figure one can see a numerical solution of the generalized KdV equation (29) augmented by the integral viscous term (30) describing a viscosity in the laminar boundary layers. For the initial condition, the experimentally recorded wave form near the wavemaker was used. Two calculations were performed, with and without viscosity. Numerical results without viscosity show a soliton formation; initial pulse amplitude gradually increases and quickly tends to a constant value, as shown by the dashed line in Fig. 14. However, when the viscosity is taken into account, the initial pulse amplitude only slightly increases and then decreases noticeably, as shown by the solid line in Fig. 14. Unfortunately, that solution was restricted due to numerical difficulties; therefore, the solid curve was terminated and continued as a broken line representing an approximate analytical solution of the disturbed KdV equation, as described by Eq. (32). One can see that experimental and theoretical data agree well. The authors note the "use of the more-accurate expression" of Ref. 10 yields even better agreement with these data (see, however, the discussion of results of Ref. 10 below).

As the viscosity affects the solitary wave amplitude, it is natural to expect that it can also affect the wavelength. However, the dissipation of linear perturbations in the laminar boundary layer linearly depends on wave number k, whereas the dispersion term in the KdV equation is proportional to k^3. This means that, for relatively large amplitude and, hence, small-wavelength solitons (we recall that for the KdV soliton, $\Delta\sim\eta_0^{-1/2}$), the nonlinear and dispersive effects prevail over dissipation. In the process of soliton damping, when its amplitude decreases due to viscosity and wavelength grows, dissipation becomes increasingly important and can eventually prevail over dispersion. Then, the adiabatic relationship for a KdV soliton, $\Delta^2\eta_0=\text{const}$, ceases to be valid. The authors of Ref. 21 found in their numerical study that there is indeed a deviation from the adiabatic relationship for small-amplitude KdV solitons: at the same amplitude, the soliton is shorter in the viscous case. (Nonadiabatic corrections to soliton shapes due to different kinds of dissipation were studied in Refs. 24 and 78.) The smaller the soliton amplitude, the more this deviation was pronounced in that experiment. The viscosity effect is insignificant for soliton amplitudes of $\eta_0/h_2>0.1$. Now the experimental data deviation from theoretical lines at small amplitudes presented in Figs. 9 and 10 can be explained by the influence of boundary-layer dissipation. The deviation remains small exactly within the predicted amplitude range $\eta_0/h_2<0.1$.

In Ref. 10 the authors derived an expression for the total rate of energy loss per unit width of tank for a KdV internal soliton in a two-layer fluid in the general case of layers of different density, viscosity, and depth. They took into account the energy loss from the lower fluid due to the bottom and wall boundary layers in the tank, in the upper fluid due to the wall boundary layers, and in the boundary layers at the interface between two fluids. The equation derived for the soliton amplitude decay in space has the same form as (32) with the same expression for the characteristic distance of soliton decay in the limit of $\Delta\rho/\rho_{1,2}\ll 1$ and $\nu_1=\nu_2$.

The authors tested the validity of their theory by comparing its predictions with the decay rate of the internal solitons observed in Ref. 22 (see the description of the experiment in Sec. III). Their results are presented in Fig. 15. The obvious discrepancy between the theory (solid line) and experimental data (triangles) were explained by the influence of "parasitic" water motions. Namely, when the internal soli-

ton was generated first, the surface waves were also produced by the same piston. Surface waves propagate faster than the internal waves and leave some residual water motion behind that is codirected with the water motion induced by the internal soliton in the upper layer. Because of that, the velocity shear is reduced in the upper layer and, as a consequence, the decay is also reduced (by about 1/3 according to the authors' empirical estimate). Meanwhile, when the soliton is reflected from the remote tank end and moves back toward the wavemaker, it propagates in a head-on direction with the residual surface and its own internally induced motion. Therefore, the velocity shear is noticeably greater than in the previous case, and the soliton decays faster. The results presented in Fig. 15 are in qualitative agreement with such an explanation (the reflection boundary at the remote end of the tank is shown in the figure). The revised theory with the empirically reduced decay rate is shown in the figure by the dashed line; the last two triangles correspond to solitons propagating toward the wavemaker after reflection from the remote tank end.

The paper by Gavrilov[80] was also devoted to the study of soliton attenuation due to viscosity. The author carefully studied this effect for different combinations of two immiscible fluids, both under rigid lid conditions and with a free surface. He used tanks of different sizes: 220 cm $\times$ 17.5 cm $\times$ 15 cm, 390 cm $\times$ 20 cm $\times$ 6 cm, and 390 cm $\times$ 6 cm $\times$ 6 cm filled with two-layer fluid: the saltwater in the lower layer ($\rho_2=1$ g/cm^3, $\nu_2=0.01$ cm^2/s), and a mixture of kerosene with khladon-113 ($\rho_1=0.9$ g/cm^3, $\nu_1=0.0141$ cm^2/s) or pure kerosene ($\rho_1=0.8$ g/cm^3, $\nu_1=0.0162$ cm^2/s) in the upper layer. To explain these data, the author slightly modified the theoretical results of Refs. 10 and 21 and found very good agreement between theory and experimental data for the dependency of the soliton amplitude on distance. The shapes of solitary waves corresponded very well to the KdV theory for rather small amplitudes ($\eta_0/H \approx 0.05$), where $H=h_1+h_2$. For larger amplitudes, the discrepancy between theory and experiment was quite noticeable. However, experimental data agreed very well, up to $\eta_0/H \approx 0.15$, with the second-order shallow-water theory developed by Ovsyannikov.[81]

B. Experimental study of waves in a rotating fluid

1. Quasiplane wave beams in a rotating fluid

In this section we discuss the results of experimental study of internal wave generation and propagation in a large rotating tank built in the "Coriolis" laboratory (LEGI, Grenoble, France).[42] The tank, 14 m in diameter and 1.2 m in height, is placed on a rotating platform whose frequency of rotation can vary in a wide range. This facility allows the modelling of important geophysical processes, including surface and internal waves in a rotating ocean.

The tank was filled with a two-layer fluid, saltwater in the lower layer, and freshwater in the upper layer. The angular velocity of tank rotation varied within a wide range. This allowed study of different regimes of fluid rotation starting from nonrotating fluid and "extremely weak" rotating to strongly rotating.

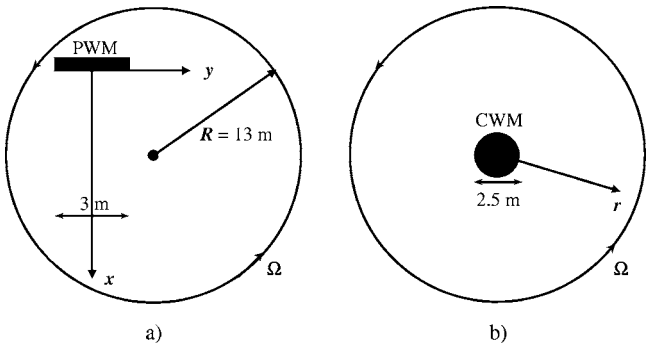

FIG. 16. Sketch of the rotating water tank equipped with the plane wavemaker (PWM) in (a) and cylindrical wavemaker (CWM) in (b).

The first set of experiments to be discussed concerns waves with approximately plane fronts [actually they represented two-dimensional (2D) wave beams].[38] Thicknesses of water layers in these experiments were $h_1=5$ cm (upper layer) and $h_2=35$ cm (lower layer). The relative density difference between the layers, $\delta\rho/\rho$, was about 0.5%. Internal waves were generated at the periphery of the tank by a plane wavemaker 3 m long and 45 cm wide [Fig. 16(a)]. The maximum wave amplitude was 1.5 cm without rotation and less than 1 cm when rotation occurred.

Prior to studying waves in a rotating fluid, the authors conducted an experiment with the generation of quasiplane internal solitary waves in a nonrotating fluid. As the wavemaker of limited width generated an internal wave beam that was not limited by sidewalls, as occurs in typical channel-type tanks, a small transversal diffraction occurred. The diffraction caused an energy leakage from the axis of the beam to the sides. In spite of such energy loss, reasonably good agreement between parameters of generated solitary waves and KdV solitons was found; the results of that experiment were considered further as reference data.

Then, the authors studied four regimes of rotation parameterized by the value of exponent q of a small parameter ε, as described in Sec. IV B 1: "extremely weak" ($q=4$), "very weak" ($q=3$), "weak" ($q=2$), and "strong" rotation ($q=1$). They did not specify explicitly the value of the rotation frequency in each particular case, but indicated that the period of rotation varied in the range 50–1000 s.

It was discovered in the experiments that, unlike the solitary waves observed in tanks with rigid walls, the interface between the leading solitary wave and the following dispersive wavetrain never comes back to the rest level, both with and without rotation. The leading solitary wave was a depression of the pycnocline, because the thickness of the lower layer in the experiment was greater than that of the upper one, $h_2 > h_1$. However, the depression was followed immediately by the pycnocline elevation of a smaller amplitude. The authors presumed that this could be due to the effective wave energy loss through the sides of the wave beam caused by diffraction. This explanation sounds reasonable because, as was shown by Gorshkov and Papko[24] and Khasanov,[78] the shape of the tail behind the soliton in dissipative media strongly depends on the type of dissipation, and for some kinds of dissipation (e.g., for Rayleigh dissipation),

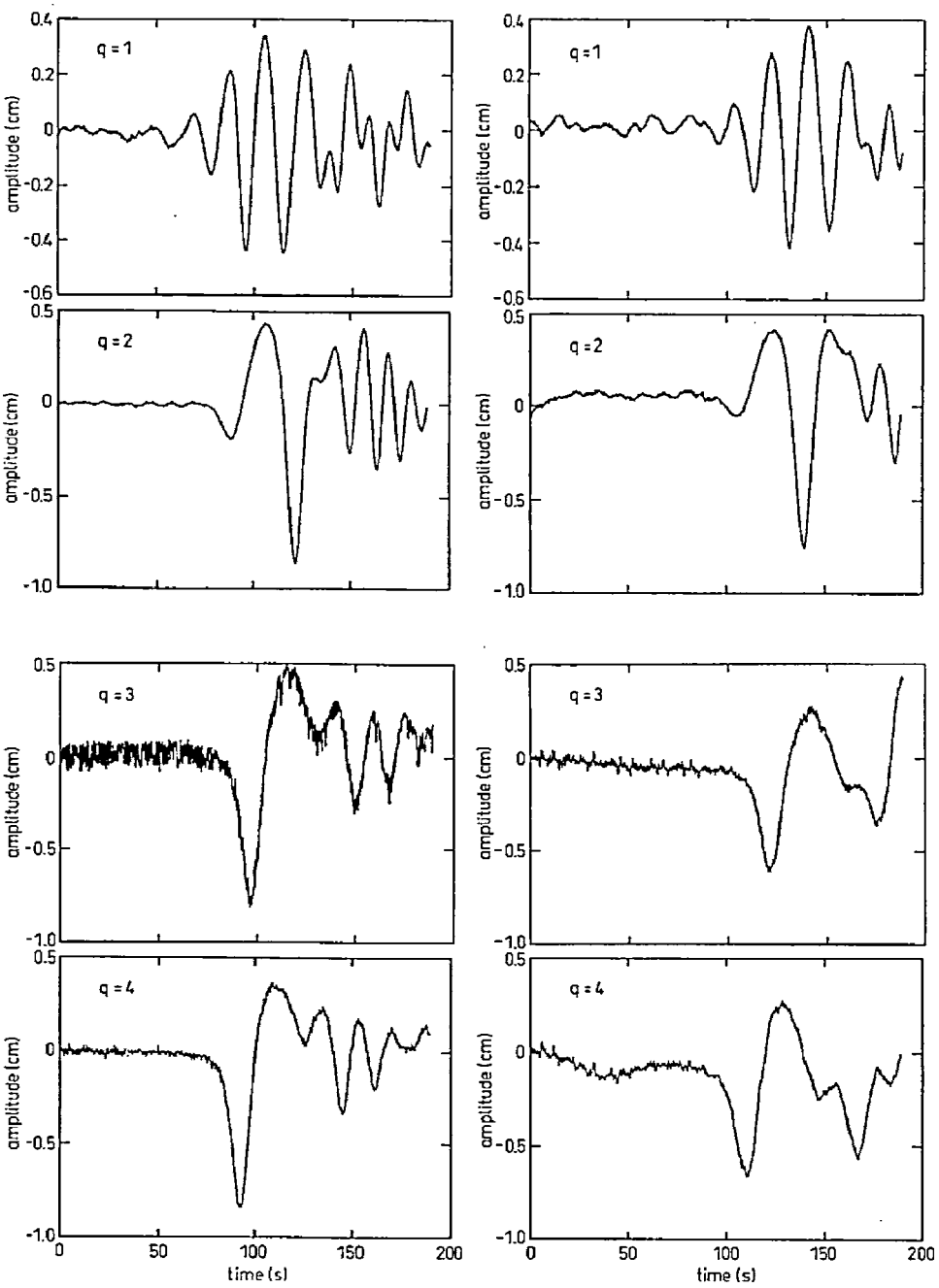

FIG. 17. Wave profiles at two distances from the wavemaker (left frames—6 m away from the wavemaker; right frames—7.2 m away from the wavemaker) for four different rotation rates: $q=1$—"strong rotation" case; $q=2$—"weak rotation" case; $q=3$—"very weak rotation" case; and $q=4$—"extremely weak rotation" case. From Ref. 38.

the perturbation immediately behind the soliton might be opposite to the soliton polarity. However, the detailed influence of energy leakage due to diffraction on the structure of a soliton tail was not studied.

In the case of extremely weak rotation, as expected, the shape of the wave closely resembled that recorded without rotation: there was a leading solitary wave of negative polarity followed by an elevation and a train of dispersive waves (Fig. 17, $q=4$). At the central zone of the wave beam the wave was quasiplane with amplitude variation within ±8% along the crest of 2.5 m length covered by several recording probes. When the rotation increases in a certain range, "the general solitary wave shape is conserved"; however, its amplitude decreases, "while the amplitude of the elevation immediately following it becomes much larger than in the nonrotating case."

For the case of very weak rotation, $(q=3)$, experimental data for the wave velocity versus amplitude for the leading solitary wave were found to be in satisfactory agreement with the theoretical prediction; i.e., they were close to that predicted by the KdV theory, Eq. (7). As mentioned in Sec. IV B 1, the only effect of rotation in this case is the appearance of a transverse component of fluid velocity that is of the next order of smallness with respect to the longitudinal component. An agreement with KdV theory was also obtained for the relationship between the solitary wave amplitude and its characteristic wavelength. Still, an agreement with the theory was much better when there was no rotation at all or when the rotation was extremely weak. It was observed that the experimental data for the dependency of characteristic wavelength Δ on amplitude η_0 were somewhat more scattered and

shifted down from the theoretical line when the rotation increases from an "extremely weak" to "very weak" value. The characteristic wavelength was defined as

$$\Delta = \frac{1}{\eta_0}\int_0^\infty \eta(x,t)dx. \tag{46}$$

Note that $\Delta = M/(2\eta_0)$, where the "wave mass" M is determined in Eq. (36); only the frontal portion of a solitary wave was used for calculation Δ to exclude the distorting influence of the tail following in the rear part of the wave.

In our opinion, in this case the authors actually observed an initial stage of the terminal decay of the KdV soliton. A limited distance did not allow observation of a complete soliton disappearance due to rotation. The circumstantial evidence of this regime is the heavy tail generated behind the solitary wave and the linearly growing background in the space in front of the solitary wave. This strongly resembles wave patterns obtained in numerical calculations of soliton terminal decay.[39]

For the higher rotation rate (the "weak rotation" case), the authors obtained very repeatable results, observing "the same distinctive equilibrium shape, with three crests evolving together in front of a tail of dispersive waves" (Fig. 17, $q=2$). The leading part of the wave had a stable shape, whereas the shape of the tail changed with the distance. The dependency of the wave speed on the solitary wave amplitude was still close to linear, although the data were more scattered than in the nonrotating or very weakly rotating cases with $q=4$ or 3.

As for the relationship between solitary wave amplitude and width, there is an ambiguity in the definition of the width due to the alternative character of the solitary wave profile even in its frontal part (see Fig. 17, $q=2$). Therefore, the results obtained by the authors do not seem to be reliable and need further examination.

The authors suggest that in this experiment they obtained experimental evidence of their analytical solution for the "Ostrovsky wave" (see Sec. IV B 1). Their opinion is based on the analysis of the relationship between solitary wave amplitude and characteristic wavelength, especially for $\Delta''(\eta_0)$: "such a relation between distances characterizing the front part of the wave supports the conclusion that this front part is a permanent feature, at least for the distance over which we measured it, i.e., between 3 and 8 m from the wave generator." In the meantime, they admit "the wave shape is not correctly described by our asymptotic solution," which does not predict a small depression pulse on the front of the main solitary wave (see Fig. 17, $q=2$).

In the case of strong rotation, a wave packet of much smaller amplitude ($\eta_0 \approx 0.5$ cm) emerged from the initial pulse generated by the wavemaker. No solitons were observed. The shape of the wave packet was "distinctly symmetrical with respect to the undisturbed interface level" (see Fig. 17, $q=1$). The velocity of the wave packet was "almost constant with x, and not related to the amplitude." Our estimates for this case with a rotation period $T_r=50$ s (which is, apparently, the "strong rotation" case) show that the Coriolis dispersion predominated over nonlinearity by more than an order of magnitude. Evidently, this case represents a linear evolution of a wave packet in a rotating medium.

In the conclusion the authors discuss several possible sources of discrepancy between the theory and their experiments. For instance, a pulse of depression with a nonzero total mass was generated by the wavemaker, which is inconsistent with Eq. (34) used for the theoretical analysis. As was already mentioned (see Sec. IV B 1), the rKdV equation (34) is valid only for initial perturbations of zero total mass (see, however, a paper by Grimshaw,[94] in which the problem of the adjustment of an initial perturbation to the zero-mass condition is studied).

Another discrepancy with the theory, which is not mentioned by the authors explicitly, is the disappearance of the first depression on the wave front at far distances from the wavemaker when the wave amplitude becomes small. According to the authors, the shape of a solitary wave in this case becomes "very similar to the computed shape" for the "Ostrovsky soliton." Meanwhile, as mentioned in Sec. IV B 1, solitary solutions approximately constructed by Renouard and Germain[38] indeed look similar to the large amplitude "Ostrovsky solitons" numerically constructed in Refs. 48 and 49, but for the case of negative β! And in contrast with the results of Ref. 38, oscillations on soliton tails appear when the soliton amplitude decreases; the smaller the amplitude, the more oscillations appear. Something similar to that was observed by Papko[82] in wave modeling in an electromagnetic LC lattice (see Ref. 3).

This classification of rotational regimes is conditional to some extent because the authors evenly notice that "the boundaries between the different regimes are not clear cut, and thus there is some overlapping of the domain of validity for the equations" describing wave propagation.

2. Cylindrical waves in a rotating fluid

Another series of experiments conducted in the same large rotating tank in the laboratory "Coriolis" dealt with cylindrical internal waves.[55] The results obtained were interpreted within the framework of a rotation-modified cKdV equation (37). A circular, piston-type paddle with an internal radius of 1.25 m was placed in the center of the circular tank [Fig. 16(b)]. This 5-cm thick, 25-cm wide cylindrical annulus moved vertically along a cylinder 2.5 m in diameter. The paddle could perform either sine-like ("periodic") motion with given numbers of oscillations or a single one-directional motion (upward or downward) with a constant speed. The amplitude E and period T_p (or a duration T_s for the single displacement) of the paddle movement could vary.

Two different ratios of the upper- to lower-layer thicknesses were chosen: $h_1/h_2=4$ and $1/4$, as well as two different values of relative density difference of the upper and lower layers, $\delta\rho/\rho \equiv (\rho_2-\rho_1)/\rho_2 = 0.35\%$ and 1%.

The amplitude and period of excitation were chosen in the ranges of $E=1-3$ cm and $T_p=10-70$ s for the "periodic" movement; and $E=3$ cm, the duration $T_s=4$ s for the upward or downward single movements. In order to obtain a reference set of data, experiments without rotation ($f=0$ rad/s) were performed; then, the weak ($f=0.058$ rad/s) and strong

($f=0.1$ rad/s) rotation cases were studied with $f=2\Omega_r=2(2\pi/T_r)$ being the Coriolis parameter related to the frequency Ω_r and period T_r of fluid rotation.

For the case of a very weak density difference, $\delta\rho/\rho=0.35\%$, the experiment was conducted in the nonrotating fluid at two rotation rates: "weak rotation," $f=0.058$ rad/s, $T_r=216$ s, and "strong rotation," $f=0.1$ rad/s, $T_r=126$ s.

The values of linear velocity of long internal waves in a two-layer approximation were $c=3.7$ cm/s for $\delta\rho/\rho=0.35\%$ and $c=6.26$ cm/s for $\delta\rho/\rho=1\%$.

In the experiments described below, the initial pulse generated by the wavemaker had a shape of one period of a sine function with a leading front of positive polarity for the interface displacement. According to the KdV theory,[2,20] in the plane case without rotation such a pulse evolves into a sequence of solitons, if the corresponding Ursell parameter is greater than the critical one, $\mathrm{Ur}_{\mathrm{cr}}=\sqrt{7}$; otherwise, it evolves into a dispersive wavetrain. For the experimental conditions, the Ursell parameter was always above the critical value. Hence, at least one soliton could be formed from the initial perturbation in the plane case without rotation. However, cylindrical divergence and especially rotation can prevent soliton creation because of an amplitude decrease due to energy spreading along the outgoing wave front. As mentioned above, even weak rotation can lead not only to a gradual decay of the soliton but also to its eventual "terminal" destruction. The rotation also modifies the number of generated solitons from the intensive initial perturbations and can even prohibit soliton formation completely.[38,40,51,83]

In the first experiment, only one period of sinusoidal perturbation was produced with the amplitude $E=1$ cm and period $T_p=60$ s. At least two solitary waves emerged from the perturbation with a heavy trailing tail behind them. Actually, it was not easy to separate solitary waves from the trailing wavetrain and, therefore, it is difficult to indicate precisely how many solitary waves were generated. The amplitude of the leading wave decreased with the distance from the paddle, and such a decrease became stronger when rotation increased. At all distances from the wavemaker, the perturbation amplitude decreased when the rotation increased.

In another experiment, the initial perturbation was produced by a single steady paddle movement downward at a distance $E=3$ cm for the time $T_s=4$ s. In the nonrotating case, at least two solitary waves emerged and separated from the train of much smaller waves. Similarly to the plane case, separation between two solitary waves increased with the distance from the paddle. Under the rotating action, such a clear separation was no longer observed. Near the wavemaker the leading solitary wave always had the largest amplitude, independently of the rotation frequency. Without rotation, as well as at very weak rotations, the leading pulse was the largest at all distances, although its amplitude gradually decreased. However, at high rotation rates the amplitude of the second solitary wave at large distances, $r>300$ cm, became larger than the amplitude of the first wave.

In all experiments, the speed of the leading wave was independent of the initial condition and of the wave amplitude, and it was always approximately equal to the phase speed of long linear interfacial waves. Without rotation, the second wave velocity was always smaller than the phase speed of long perturbations. When rotation is introduced, the velocity difference between the first and the second waves diminished and eventually, in the strong rotation case, two solitary waves moved with the same speed. Apparently, this indicates that the nonlinearity was not suppressed by strong rotation.

TABLE I. Damping exponent σ of the leading pulse for various experimental conditions. Regime 1: $E=1$ cm, $10\ \mathrm{s}\leqslant T_p\leqslant 70$ s; regime 2: $E=4$ cm, $T_s=4$ s.

	$\delta\rho/\rho=0.35\%$		$\delta\rho/\rho=1\%$
f (s^{-1})	Regime 1	Regime 2	Regime 1
0	$\sigma=-2/3$	$\sigma=-2/3$	$\sigma=-1$
0.058	$\sigma=-2$	$\sigma=-2$	$\sigma=-1$
0.1	$\sigma=-4$	$\sigma=-4$	$\sigma=-2$

For the first wave the characteristic wavelength was measured against wave amplitude. For the nonrotating and weakly rotating cases, the same dependency as that predicted by the KdV theory for plane solitons, $\Delta\sim 1/\sqrt{\eta_0}$, was obtained. In the strong rotation case, the wavelength was independent of the amplitude, similar to plane waves in the experiment by Renouard and Germain[38] described above; this indicates again that the linear regime took place in this case.

A decrease of the first solitary wave amplitude with distance was studied for both aforementioned regimes of wave generation, i.e., when the wavemaker performed one period of sinusoidal motion (regime 1) and when it displaced steadily downward (regime 2). The power-type approximation of pulse amplitude versus distance was used, i.e., it was assumed that $\eta_0(r)\sim r^{\sigma}$. Results obtained for the damping exponent σ of the amplitude of the leading wave for various experimental conditions are presented in Table I.

In the nonrotating case for both regimes of generation, solitary waves appeared at the leading edge of the wavetrain and decreased with distance, in agreement with the theory for KdV solitons, $\eta_0\sim r^{-2/3}$ (see previous).

Under the influence of rotation, the damping of the leading wave was stronger, and the decay exponent equaled to $\sigma=-2$ for the weak rotation and $\sigma=-4$ for the strong rotation. In Fig. 18(a) one can see the dependency of the first wave amplitude on distance for the particular case of wave generation (regime 1) with the period $T_p=70$ s and amplitude $E=1$ cm.

To illustrate the robustness of the theoretical model—the rotation modified cKdV equation (37)—to describe wave dynamics in a cylindrical rotating system adequately, two limiting cases of rotation were studied numerically within the framework of that equation:

(i) the nonrotating case with the strong density difference, $\delta\rho/\rho=1\%$; and
(ii) the strong rotation case, $T_r=126$ s, with the small density difference, $\delta\rho/\rho=0.35\%$.

The boundary conditions for these computations were taken from the real laboratory experiment, as recorded by the

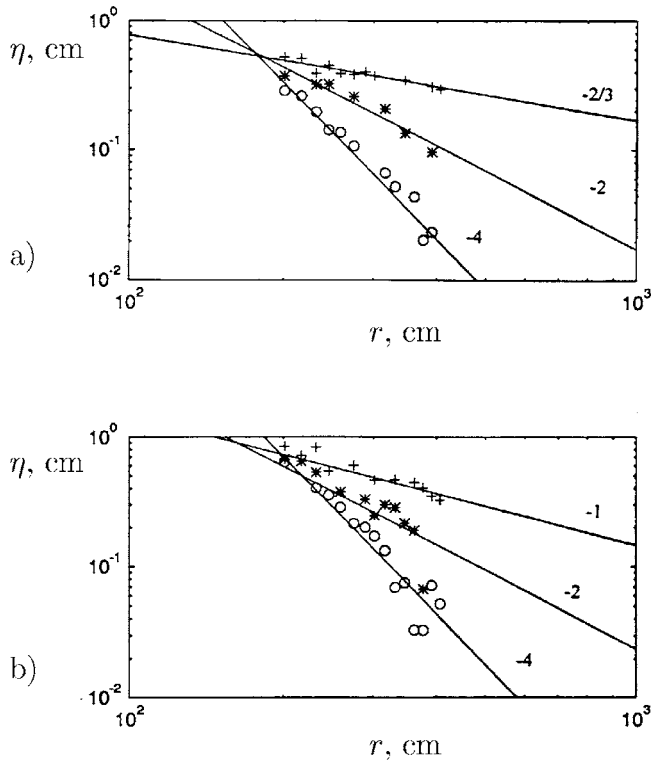

FIG. 18. First wave amplitude versus distance in the logarithmic scale for the periodic wave excitation. (a) Weak density difference, $\delta\rho/\rho=0.35\%$, $T_b=70$ s. (b) Stronger density difference, $\delta\rho/\rho=1.0\%$, $T_b=45$ s. Pluses—$f=0$ rad/s; stars—$f=0.058$ rad/s; circles—$f=0.1$ rad/s. From Ref. 55.

first probe located at a distance of 201 cm from the center of the tank (curves *a* in Figs. 19 and 20). The subsequent frames, (b)–(e), show the records of the interface displacement and corresponding numerical results for different distances: (b) 245 cm; (c) 259 cm; (d) 302 cm; (e) 361.5 cm.

As one can see from these figures, there is fairly good agreement between experimental (thin lines) and numerical (thick lines) data. Some discrepancy between these data can be explained by the influence of dissipation, turbulence, and other side factors that always present in the real experiment but was ignored in the computations. Another source of discrepancy may be linked to the relatively small distances of wave registration points from the center of the tank, whereas the cKdV equation is formally valid at large distances from the center. For the particular experimental conditions this requires $r \gg 50$ cm.

A comparison of these two figures shows a qualitative difference in the evolution of the initial perturbation in rotating and nonrotating fluids. In the latter case, Fig. 19, one can see a pronounced leading pulse followed by a nonstationary wavetrain. The frontal part of the pulse is close to the KdV soliton. The pulse amplitude gradually decreases. In the former case, Fig. 20, the perturbation evolves into an essentially nonstationary wavetrain. The amplitude of the leading wave decreases very fast while the wave maximum shifts to the rear and slowly decreases. Moreover, at short distances from the center, the global maximum of the wavetrain can even increase because of the energy transformation from the front to the back of the wavetrain.

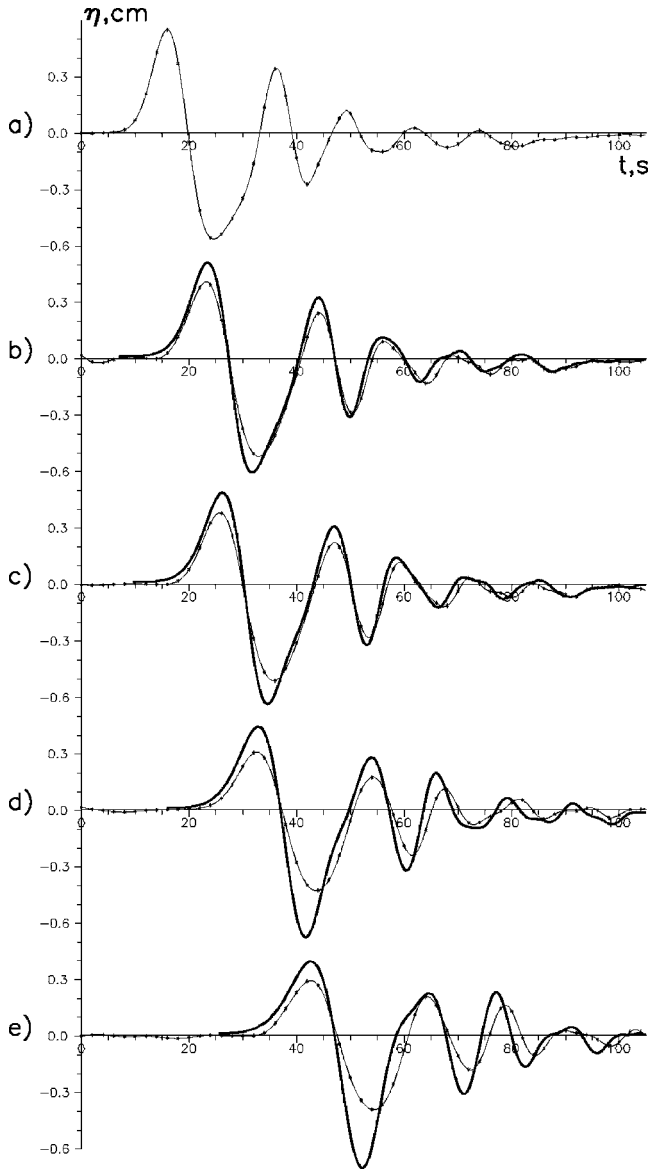

FIG. 19. Comparison of experimental data (thin lines) with numerical results (thick lines) for the internal wave in a cylindrical system without rotation. From Ref. 55.

To study the influence of the rotation effect on the decay of outgoing pulse perturbation, an additional numerical computation was conducted within the framework of Eq. (37). The initial pulse was chosen in the form of one period of sinusoidal perturbation, similar to that generated in the experiment described above. Parameters for the equation coefficients were calculated from the hydrological experimental data.

It was determined that the pulse evolves into the wavetrain that decays with the distance in a fairly complex way (see Fig. 21). The amplitude of the leading edge of the wavetrain (the first wave amplitude) decays much faster than the global wavetrain amplitude (cf. the data around lines 1 and 2 in Fig. 21). Both of them decay, apparently, in a nonpower manner. However, at small distances, separate limiting pieces of line 1 might be misinterpreted as a power-type

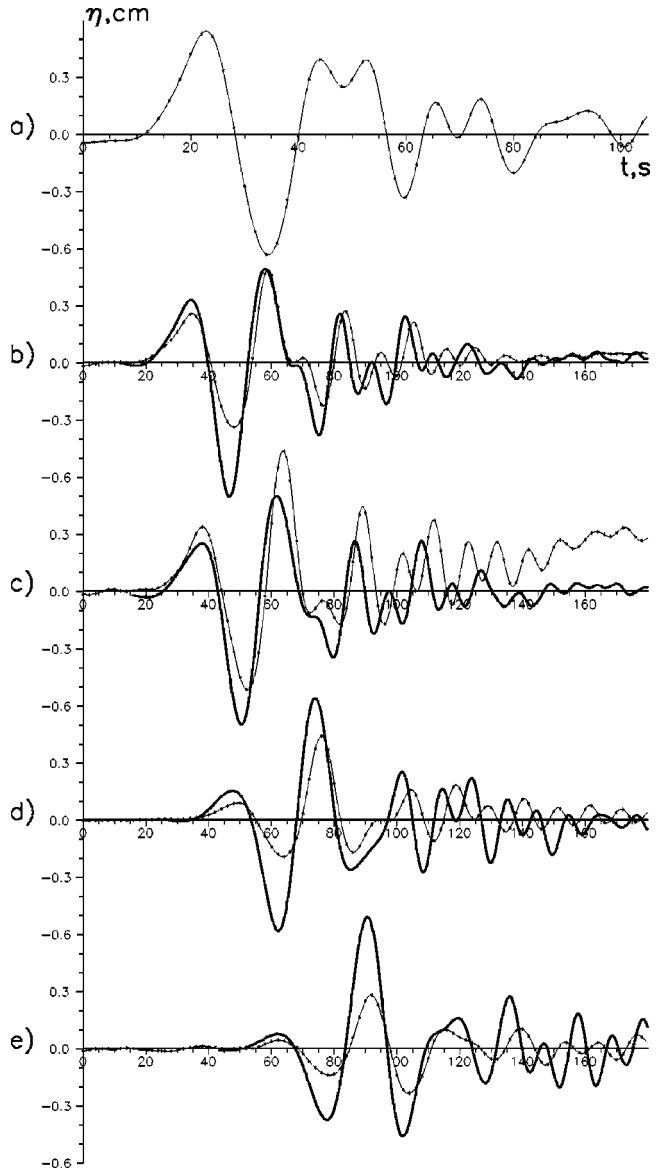

FIG. 20. Same as in Fig. 19 but with strong rotation, $T_r=126$ s. From Ref. 55.

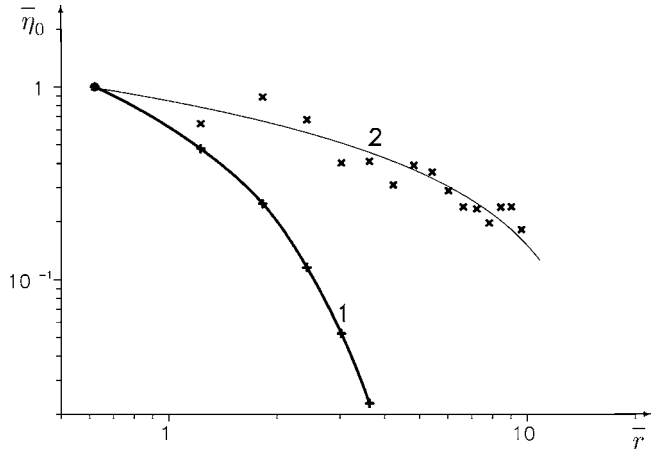

FIG. 21. Dependencies of the leading wave (pluses) and maximum of wavetrain (crosses) on distance in normalized variables. From Ref. 55.

decay $\eta_0 \sim r^{\sigma}$ with different exponents, $\sigma=-1$, -2, -3, or even -4. Perhaps this explains the variety of experimentally obtained exponents presented in Table I.

The results obtained can be summarized as follows:

(1) without rotation, the experimental data are in very good agreement with the results obtained by different authors for the cylindrical KdV solitons. This involves the phase speed, wavelengths, and soliton damping rate;
(2) when the rotation is introduced, there are important changes, some of them in agreement with the previous experimental observations[38] and numerical studies.[51,83] It involves a decrease in the number of solitons generated from the initial perturbation and the destructive action of rotation on KdV solitons. In particular, the damping rate of the first wave increases with an increase of the rotation rate. In addition, it was found that the amplitude of the second wave tends to become larger than the amplitude of the first wave when the distance increases. Apparently, this indicates the formation of a quasilinear wavetrain.

C. Solitary waves of large amplitudes in laboratory experiments

As was mentioned in Sec. III, in the pioneering experiment by Davis and Acrivos in 1967,[16] large-amplitude internal solitary waves of the second mode were observed. It was demonstrated that such billows can contain vortex cores with water trapped inside so that they can transport not only energy and momentum but also mass. However, quantitative characteristics of billows were not studied in detail at that time.

Another experiment in which strongly nonlinear IWs were observed was performed by Yates in 1978. His paper is cited by Koop and Butler in Ref. 21 but, unfortunately, we were unable to obtain its copy. According to Ref. 21, Yates experimented with internal waves of large amplitudes in a continuously stratified fluid.

Strongly nonlinear solitary waves were then studied by Miyata,[71] who performed a laboratory experiment to verify the solitary solution obtained within the framework of his long-wave theoretical model mentioned previously in the theoretical part. Experiments were carried out in a glass tank 180 cm $\times$ 30 cm $\times$ 7 cm. Two types of immiscible fluids were used in the study: (i) freshwater ($\rho_1=0.999$ g/cm^3) and aniline ($\rho_2=1.02$ g/cm^3), and (ii) oil ($\rho_1=0.87$ g/cm^3) and freshwater ($\rho_1=0.999$ g/cm^3). In both cases the results obtained were very similar. Solitary waves propagating along the density interface were photographed by two cameras and then plotted against theoretical curves. Several depth ratios were used so that upper-layer thickness varied from 10 to 20 cm and lower layer thickness, from 1.3 to 1.5 cm. Solitary-wave amplitudes ranged from 0.9 to 2.2 cm.

Figure 22 taken from Ref. 71 illustrates a comparison of theoretical and experimental data. The ratio of soliton amplitude to the thickness of the lower layer was greater than 0.64 in the experiment, so that the nonlinearity was very strong. As seen from Fig. 22, experimental data (dots) agree very

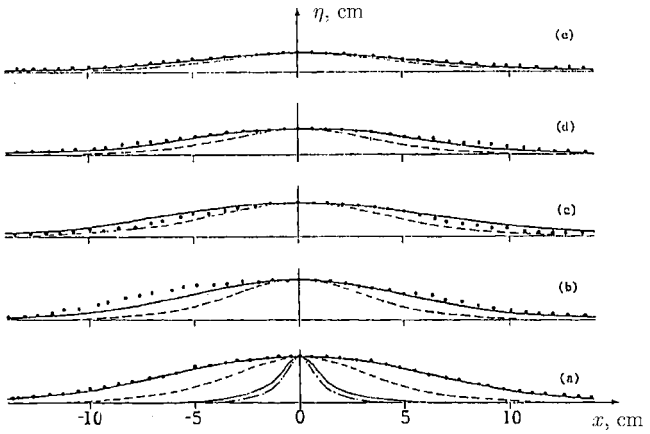

FIG. 22. Comparison of theoretical and experimental data for large-amplitude solitons. Dots are experimental points. Solid line—solitary wave from Miyata's long-wave model; dashed line—KdV soliton; thin solid line—BO soliton; dot-dashed line—JKKD soliton. The latter two theoretical profiles are not shown in (b)–(e), but they are below the KdV profile. $\zeta(\xi)$ is equivalent to our $\eta(\xi)$, where $\xi=x-Vt$. (a) $\eta_0/h_2=1.57$; (b) $\eta_0/h_2=1.27$; (c) $\eta_0/h_2=1.14$; (d) $\eta_0/h_2=0.92$; (e) $\eta_0/h_2=0.64$. From Ref. 71.

well with Miyata's nonlinear model (solid line) in the full range of amplitude ratios. As mentioned above, the latter model is essentially the same as the system (40)–(42). KdV theory (dashed line) approximates experimental data more or less well only for the minimal amplitude ratio, $\eta_0/h_2=0.64$ (in that particular experiment). The stronger the nonlinearity, the poorer the agreement between experimental data and the KdV model, whereas Miyata's nonlinear model works well even for large amplitudes [see Fig. 22(a)].

Soliton shapes predicted by other models, BO (thin solid line) and JKKD (dashed-dotted line) are also far from the experimental data. This is not surprising because both these models are valid only for weakly nonlinear cases disregarding the other limitations (the BO model is applicable for the case when one of the layers is infinitely deep; the limitations of the JKKD model were discussed above). More surprising is that the KdV model is again the most robust.

The results of this experiment also agree with other strongly nonlinear theoretical models discussed above. Indeed, Miyata's model is equivalent to the Choi-Camassa model, and for the depth ratios, h_2/h_1, lying between 6 and 12, both the beta- and Choi-Camassa models give close results.

Miyata's experimental results were later augmented by Michallet's and Barthélemy's numerical and experimental data.[73] Their laboratory tank of approximate dimension 300 cm$\times$15 cm$\times$10 cm was filled with two immiscible fluids: petrol ($\rho=0.78$ g/cm^3) and water ($\rho=1.0$ g/cm^3). Due to a relatively large density difference, the rigid lid approximation is not valid for this case, and the authors compared their results with free surface theory. The main goals of that study were to examine the characteristics of interfacial solitary waves for a wide range of layer thickness ratios and to focus on properties of large-amplitude solitary waves. There, the term "large-amplitude" related to waves whose amplitudes are comparable with the difference between the real position of the pycnocline, h_1 (or the thickness of the upper layer), and its critical position, h_c, when the coefficient of quadratic nonlinearity, α, vanishes [see Eq. (9)], i.e., to waves having amplitudes $\eta_0|h_1-h_c|$. Two main characteristics of solitary waves were tested versus amplitude: the wave velocity, V, and "frequency" Ω_s, the quantity inverse proportional to the pulse duration, $\Omega_s=V/\Delta$, where Δ is defined in Eq. (46). Figure 23 illustrates the dependency of Ω_s on η_0/H for free surface and rigid lid conditions, where $H=h_1+h_2$ is the total depth of the fluid. It clearly demonstrates a nonmonotonous dependency of soliton "frequency" (duration) on its amplitude, predicted both by the eKdV equation and as Miyata's model.[70–72]

The above results can be summarized as follows. There was good agreement between the experimental data and theoretical prediction within the framework of the KdV model for very small wave amplitudes, $0.01<\eta_0/H<0.05$. This finding was valid for all layer thickness ratios. Larger solitons were found to be in satisfactory agreement with the eKdV model, even when the pycnocline position was relatively far from the critical one; we remind the reader that the actual validity of this equation is at $|h_1-h_c|/h_1\ll 1$. When this condition is fulfilled, it was found that the eKdV model gives a very good prediction for all amplitudes of solitary waves. The authors also carried out a fully nonlinear numerical integration of the Euler equation for steady-state solitary waves, as suggested by Miyata,[70–72] and found very good agreement between predicted and measured data for all depth ratios and for all values of solitary wave amplitudes.

In 1995 Stamp and Jacka published a paper[84] in which they reported the results of an experimental investigation of the second-mode solitary waves propagating on a thin interface between two deep layers of different densities. Their configuration was similar to that used by Davis and Acrivos[16] in their pioneering paper. Freshwater of density $\rho_1=0.9982$ g/cm^3 was in the upper layer, and saltwater, the density of which varied from $\rho_2=1.0501$ g/cm^3 to 1.1997 g/cm^3, was in the lower layer. A glass tank used in the experiment was 180 cm long, 15 cm wide, and 28 cm deep. The pycnocline located at the middle of the depth was approximated by the hyperbolic tangent: $\rho(z)=\rho_0-\delta\rho\tanh[(z-z_0)/d]$ with the characteristic thickness $d=2.5$ mm. The ratio of the total fluid depth to the effective thickness of the pycnocline $2d$ was 56. A special generation technique was used to produce single large-amplitude waves similar to those generated in the Davis and Acrivos experiment.[16] The authors observed solitary waves of maximum amplitude $\eta/d=3.75$; however, the technique allows production of waves up to at least $\eta/d=5$.

In the process of propagation of large-amplitude solitary waves, their gradual decay was observed after reflections from the faceplate walls and several traverses of the tank. The authors found that "the large-amplitude waves had both laminar and turbulent regions: along the open streamlines the flow was laminar and fluid stratified, whereas within the closed streamline region the flow was turbulent and the fluid well mixed." Eventually the large-amplitude solitary wave decreased, lost its turbulent core, and transformed into a small-amplitude wave with open streamlines whose shape was very close to a BO soliton similar to that shown in Fig.

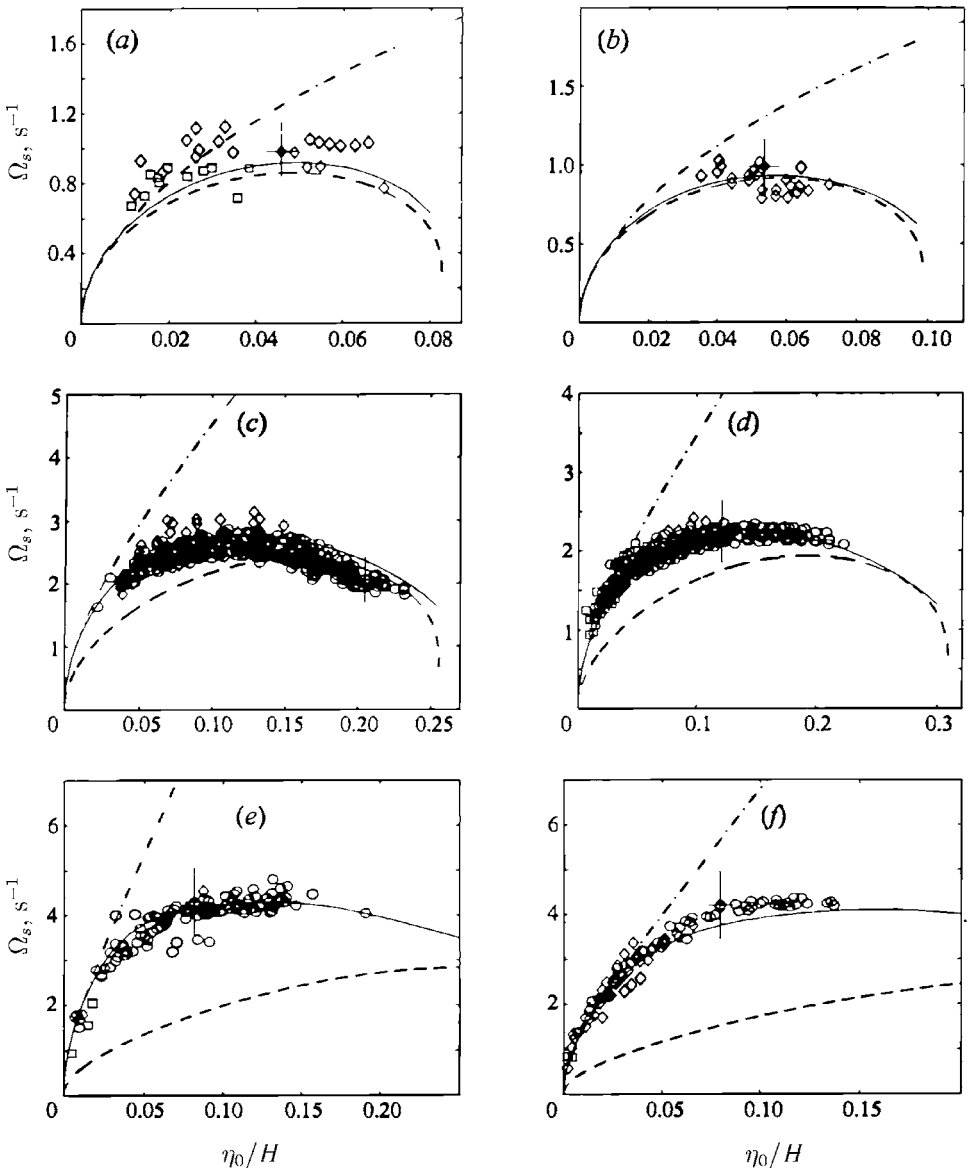

FIG. 23. Characteristic "frequency" of solitary wave, Ω_s, versus amplitude η_0. Different symbols stand for the incident wave, once reflected wave from the sidewall of the tank and twice reflected wave from two walls. The solid line is a numerical calculation from the fully nonlinear two-layer model; the dashed line represents eKdV dependency for a solitary wave; the dash-dotted line represents the usual KdV dependency. Frames (a), (c), and (e) for free surface condition; frames (b), (d), and (f) for the rigid lid condition. (a) $h_2/H=0.4$; (b) $h_2/H=0.63$; (c) $h_2/H=0.77$; (d) $h_2/H=0.84$; (e) $h_2/H=0.91$; (f) $h_2/H=0.09$. (For details see Ref. 73.)

5 from Ref. 17. The asymmetry of wave profiles with respect to the mid-pycnocline level also has been found both for small- and large-amplitude waves similar to that in the photos shown in Ref. 16. The authors assume that it might be caused by the non-Boussinesq effects and/or the difference in the free upper boundary condition and fixed lower boundary.

Since the wavelength–amplitude relationship for solitary waves provides a simple accurate basis for comparing experimental data with theoretical predictions, the authors attempted to make measurements for the entire range of amplitudes. However, they failed to obtain accurate results for small-amplitude waves and to determine the functional dependency between the wavelength and the amplitude. In the meantime, results obtained for large-amplitude waves were fitted by linear dependency $\Delta=0.95d+2.1\eta_0$ within the amplitude range $1.0\leqslant\eta_0/d\leqslant3.1$. Note that this linear dependency is quite different from the monotonically decreasing dependency, Eq. (25), for small-amplitude BO solitons. A similar nonmonotonic relationship between the wavelength and amplitude is already well known for eKdV solitons (see Fig. 3). A new important and interesting finding is that "all waves of amplitudes $\eta_0/d\geqslant1$ are similar in shape and differ only by a scaling factor." This observation correlates with the numerical results of Pullin and Grimshaw,[85] who found that for limiting wave amplitudes in the deep fluid, $\Delta\to2.18\eta_0$.

The authors also determined wave-speed–amplitude dependency for solitary wave amplitudes within the range $0.1\leqslant\eta_0/d\leqslant3.1$. They supplemented their data with the results obtained by Davis and Acrivos[16] and fitted all combined data by straight line $V/c=1.0+0.49\eta_0/d$. This can be compared with the corresponding dependency for small-amplitude BO solitons given by Eq. (25). Then they came to the conclusion that "the weakly nonlinear theory is accurate at small amplitudes, $\eta_0/d<0.5$; however, at large amplitudes the measurements [of the wave speed] are underestimated" by the prediction of weakly nonlinear theory. Meanwhile, a numerical solution obtained by Tung *et al.*[86,87] for the interfacial waves of the second mode at a similar stratification, "is in excellent agreement with measurements over the entire range of amplitudes" (see, also, a more general theory presented by Turkington *et al.*[87]).

Other features of large-amplitude waves in deep fluid were also studied, including wave attenuation, wave–wave interactions, and reflection from a solid vertical boundary. It was found that "the attenuation was independent of amplitude" and the amplitude decreased linearly with distance. However, the authors admit that "further work is required" for the understanding of wave attenuation.

In another study of large-amplitude solitary waves accomplished by Grue *et al.* in 1999,[63] a precise technique was used to examine different characteristics of solitary waves against the theory. The wave tank was 50 cm wide and of three different lengths: 620, 1230, and 2140 cm. The total fluid depth varied between 38.5 cm ($h_1=7.5$ cm, $h_2=31.0$ cm) and 77 cm ($h_1=15.0$ cm, $h_2=62.0$ cm), so that in both cases the h_2/h_1 ratio was 4.13. Fluid stratification was represented by two miscible layers: saltwater of density $\rho_2=1.022$ g/cm^3 in the lower layer, and freshwater of density $\rho_1=0.999$ g/cm^3 in the upper layer. The thickness d of the pycnocline ranged from $0.13h_1$ to $0.26h_1$. In the experiments the particle velocity as well as wave velocity and soliton shape were measured by means of particle tracking velocimetry (PTV). The results obtained were compared with the KdV theory and a fully nonlinear model for the two-layer fluid mentioned above. The latter model is based on the exact representation of two-dimensional hydrodynamic equations in the integral form with the rigid lid approximation. The wave velocity and profile can be obtained by numerically solving integral equations of the Fredholm type of the second kind.

Theoretical predictions within the KdV equation agreed well with the results of a fully nonlinear model when soliton amplitudes were relatively small, $\eta_0/h_1<0.4$. In the experiment at $\eta_0=0.4$, the deviation of soliton velocity from the value predicted by the KdV theory was about 50%. For larger amplitudes the exact theory predicts much wider solitons than follows from the KdV model. These results agree well with Miyata's long-wave model and evolution equations discussed above.

Good agreement between experimental data and numerical results obtained within the framework of a strongly nonlinear model was found both for the propagation velocity and the shape of a soliton. Normalized solitary wave amplitudes, η_0/h_1, varied between 0.4 and 1.51; the latter value is rather close to the limiting soliton amplitude, which amounts to $\eta_{\max}/h_1=1.56$. The calculated vertical profiles of the horizontal velocity component, $u_x(z)$, in both layers also agreed well with measurements performed for wave amplitudes ranging from $0.22h_1$ to $1.45h_1$. A comparison of theoretical dependencies of horizontal particle velocities on wave amplitude for the fully nonlinear theory showed that it remains robust within a wide range of depth ratios, h_2/h_1, up to 100 (in the experiments, the depth ratio was 4.13). This agrees with the experimental observations by Kao, Pan, and Renouard.[18] With regards to average horizontal velocities in each layer, they are very well approximated by Eqs. (43). As already mentioned, this is due to the mass conservation that for long waves (when the velocity is almost horizontal, and exactly horizontal at the crest) gives the same result independently of the applicability of any specific model.[75]

Unfortunately, no experimental data were obtained for the wave velocity for amplitudes less then $0.4h_1$. For this minimally measured soliton amplitude, $\eta_0=0.4h_1$, the disagreement of experimental data with the KdV theory prediction is already about 50%. The larger the wave amplitude, the better the agreement with Miyata's theory for the wave profile. However, near-limiting solitons whose amplitudes were close to the predicted maximum value, $\eta_0/h_1=1.55$, Eq. (39), deviated from the theoretical shape in the rear part of their profiles. They produced strong horizontal velocity shear between upper and lower layers so that the Kelvin–Helmholtz instability occurred, and that was the cause of the wave profile distortion. The authors of Ref. 63 estimated that a strong solitary wave with an amplitude $\eta_0=1.45h_1$ produces a shear flow with the local Richardson number, Ri $=0.07$. Meanwhile, in accordance with the theory of hydrodynamic stability, in the cases when Ri was greater than 0.25, the instability was not observed in the experiment.

Note that in Miyata's experiments, the maximum value of the relative soliton amplitude, η_0/h_2, was about 1.57 [see Fig. 22(a)]. This value was far enough from the limiting value, which is 4.89 according to Eq. (39). Therefore, the hydrodynamic instability was not observed by Miyata.

A further laboratory study of strong solitons was carried out by Grue *et al.*[88] They used the same tank as in Ref. 63, and the optical registration (PTV and PIV methods) was again employed. Note that the Reynolds numbers in these experiments were rather large, $\mathrm{Re}\sim 10^4$ and more (whereas, e.g., in the experiments by Stamp and Jacka[84] it was less than 100). Stratification was more complex; namely, the upper layer was stratified with an approximately constant buoyancy frequency, and the solitons were always observed as excursions into a lower layer with constant density, independently of the layer depth ratio. The authors excited waves of up to extremely strong nonlinearity and observed trapped cores and complex breaking and broadening phenomena with a vorticity generation. Some of the observed phenomena (but not breaking) are well described by their fully nonlinear two-layer model.

To conclude this section, the experiment by Melville and Helfrich[89] should be mentioned in which they modeled nonsteady internal waves in a two-layer fluid with a transcritical flow over topography simulated by a body moving in the upper layer (which was a rough two-dimensional analog of the Nansen's ship). The tank length was 15 m; the layer thicknesses (in our notations) were $h_1=3$ cm and $h_2=12$ cm; and the corresponding densities were $\rho_1=0.8$ g/cm^3 and $\rho_2=0.986$ g/cm^3. The experiments were compared with the forced KdV and eKdV models (i.e., equations having external terms on the right-hand sides, which model body motion). Satisfactory agreement with the observations was found for the depth ratio $h_1/h_2=1:2$, and poor agreement was found when the ratio was 1:4.

From the models discussed above, it is understandable that the larger the depth ratio, the less applicable are the long-wave models and the more nonlinear are the limiting-amplitude solitons. Grue *et al.*[90] performed a fully nonlinear numerical simulation of the experiment described in Ref. 89 and found good agreement with the experiments at a depth

ratio of 1:4, including the generation of soliton-like groups. They also found that strong nonlinearity at the site of wave generation affects the subsequent wave propagation, even at the weakly nonlinear stage.

VI. CONCLUSIONS

Laboratory experiments with internal waves allow, on the one hand, verification of the existing theoretical models and, on the other, extrapolation of the results obtained in controlled conditions, to the corresponding natural phenomena. They have already provided us with a great deal of valuable information regarding solitary waves in various situations. The experiments have confirmed that existing theoretical models often describe properties of solitary waves fairly satisfactorily, although different models are not equally robust. Some of them, e.g., the KdV model, provide good qualitative and even quantitative predictions, sometimes even beyond their formal range of validity, whereas other models, e.g., the JKKD, have narrower ranges of validity and fail to make good predictions beyond these ranges.

Overall, the following can be concluded.

- When compared with experimental data for moderate-amplitude solitons, the simple KdV model proves to be surprisingly robust, sometimes well beyond the assumed range of its formal validity. Meanwhile, experimental data obtained by different authors show a fairly large variation in the range of validity of this model. In some papers, good agreement between theory and experiment was obtained up to $\eta_0/h \approx 0.7$, whereas in others the agreement was good only when $\eta_0/h < 0.2$.
- The more advanced eKdV model provides better prediction of solitary wave parameters in cases when the pycnocline is located close to the critical position. In these cases, this model is quite relevant up to the waves of limiting configuration, as described by Eq. (16), with ν close to unity. In turn, the KdV model approximates experimental data much better in the small-amplitude limit (see Fig. 23).
- The two-layer model is simple and attractive and it works well in many realistic cases. However, for miscible fluids when the pycnocline is relatively wide, it should be used with a certain precaution. Apparently, even in the case of a wide pycnocline, an effective two-layer model can be constructed which provides the same coefficients for the KdV equation as the exact theory based on the boundary-value problem for a continuously stratified fluid, Eq. (2). However, the required parameters of the equation are not known in advance; therefore, the two-layer models usually used are not adjusted properly to the real hydrology in the experiment. As a result, only more or less good approximate estimates for the soliton parameters are possible.
- The ranges of validity of both the JKKD and BO models are not yet well verified in laboratory experiments. Hence, these models should be applied to the interpretation of ocean observations with caution.
- The shapes of small-amplitude solitary waves are not very sensitive to the model chosen. Therefore, taking into account the errors in experimental measurements, it is not easy to use wave profiles for identification of the most relevant theoretical model unless very precise experiments are carried out.
- The fully nonlinear models typically agree very well in many details with experimental observations of solitary waves. On the other hand, the simplified long-wave, strongly nonlinear models are also applicable in a rather wide range of the parameters of strong solitons, although they may need verification by comparison with numerical solutions obtained within the framework of fully nonlinear models.
- The dissipation of solitary waves in laboratory conditions is usually relatively weak, so that the nonlinear and dispersive effects remain almost in balance during solitary wave propagation. Therefore, in spite of energy dissipation, the relationship between the amplitude and characteristic wavelength of a weakly nonlinear solitary wave may remain close to that theoretically predicted for KdV solitons.
- The main mechanism of dissipation in the laboratory conditions is apparently related to laminar boundary layers on walls, bottom, and at the interface between layers of different density in the tanks. The theoretical results for this case agree well with experimental and numerical data.
- The experiments in rotating tanks confirm the theoretical prediction that the rotation can radically change the nonlinear internal wave evolution. Specifically, Coriolis dispersion caused by fluid rotation may play an important role and, in particular, can prevent the formation of well-defined solitons. Meanwhile, the existing models such as the plane and cylindrical rKdV equations are capable of adequately describing nonlinear processes observed in the plane and cylindrical systems, respectively, with rotation.

The extrapolation of laboratory results to natural conditions does, strictly speaking, need a similarity in basic dimensionless parameters such as Froude and Reynolds numbers. This is not always possible, especially with respect to the Reynolds number (even the physical nature of dissipation can be different). Meanwhile, as usually occurs in physics, the more we know, the more new questions arise. We believe that new laboratory experiments with internal waves will be conducted in the near future. As an example, special laboratory experiments in which turbulence is created can be recommended that could prove to be more relevant to internal waves in the natural environment.

In this review we did not access and discuss all aspects of solitary wave studies in laboratory conditions. For instance, solitary wave generation by tidal flow (see, e.g., Ref. 91), shoaling (see, e.g., Ref. 35) or interaction with bottom topography (see, e.g., Ref. 92) remain beyond the scope of our consideration. Here we focused on the experiments that can be considered as a validation of known long-wave models. Some additional material regarding large-amplitude internal soliton generation and propagation both in laboratory and natural conditions is discussed in the review paper by Grue[93] included in this focus issue of the journal.

ACKNOWLEDGMENT

The authors are grateful to the referees for their remarks as well as useful and encouraging advice.

[1]B. Franklin, "Behavior of oil on water. Letter to John Pringle. Philadelphia, Dec. 1, 1762," in *Experiments and Observations on Electricity*, London, 1769, pp. 142–144.
[2]M. J. Ablowitz and H. Segur, *Solitons and the Inverse Scattering Transform* (SIAM, Philadelphia, 1981).
[3]L. A. Ostrovsky, "Nonlinear internal waves in the ocean," in *Nonlinear Waves*, Proceedings of IV Gorky School on Nonlinear Waves, 1979, pp. 292–329 (in Russian).
[4]R. Grimshaw, "Internal solitary waves," Chap. 1 in the book *Environmental Stratified Flows*, edited by R. Grimshaw (Kluwer Academic, New York, 2002), pp. 1–27.
[5]L. A. Ostrovsky, "Nonlinear internal waves in a rotating ocean," Okeanologia **18**, 181–191 (1978) (in Russian) [English translation: Oceanology (Engl. Transl.) **18**, 119–125 (1978)].
[6]L. A. Ostrovsky and Yu. A. Stepanyants, "Do internal solitons exist in the ocean?," Rev. Geophys. **27**, 293–310 (1989).
[7]J. R. Apel, L. A. Ostrovsky, Y. A. Stepanyants, and J. F. Lynch, "Internal solitons in the ocean," Technical Report WHOI-05, 2005. See also http://www.whoi.edu/science/
[8]L. R. Walker, "Interfacial solitary waves in a two-fluid medium," Phys. Fluids **16**, 1796–1804 (1973).
[9]T. Kakutani and N. Yamasaki, "Solitary waves on a two-layer fluid," J. Phys. Soc. Jpn. **45**, 674–679 (1978).
[10]C. Leone, H. Segur, and J. L. Hammack, "Viscous decay of long internal solitary waves," Phys. Fluids **25**, 942–244 (1982).
[11]G. H. Keulegan, "Characteristics of internal solitary waves," J. Res. Natl. Bur. Stand. **51**, 133–140 (1953).
[12]R. Grimshaw, E. N. Pelinovsky, and T. G. Talipova, "The modified Korteweg–de Vries equation in the theory of large-amplitude internal waves," Nonlinear Processes Geophys. **4**, 237–250 (1997).
[13]T. G. Talipova, E. N. Pelinovsky, K. Lamb, R. Grimshaw, and P. Holloway, "Cubic nonlinearity effects in the propagation of intense internal waves," Dokl. Akad. Nauk SSSR **364**, 824–827 (1999) (in Russian) [English translation: Dokl. Earth Sci. **365**, 241–244 (1999)].
[14]M. Funacoshi and M. Oikawa, "Long internal waves of large amplitude in a two-layer fluid," J. Phys. Soc. Jpn. **55**, 128–144 (1986).
[15]R. Grimshaw, E. Pelinovsky, Y. Stepanyants, and T. Talipova, "Modeling internal solitary waves on the Australian North West Shelf," Mar. Freshwater Res. (to be published). See also preprint 05–05, Loughborough University, Department of Mathematical Sciences, 15 pages; website: http://www.lboro.ac.uk/departments/ma/preprints/papers05/05–05abs.html
[16]R. E. Davis and A. Acrivos, "Solitary internal waves in deep water," J. Fluid Mech. **29**, 593–607 (1967).
[17]T. W. Kao and H. P. Pao, "Wake collapse in the thermocline and internal solitary waves," J. Fluid Mech. **97**, 115–127 (1979).
[18]T. W. Kao, F.-Sh. Pan, and D. Renouard, "Internal solitons on the pycnocline: Generation, propagation, and shoaling and breaking over a slope," J. Fluid Mech. **159**, 19–53 (1985).
[19]J. Gan and R. G. Ingram, "Internal hydraulics, solitons and associated mixing in a stratified Sound," J. Geophys. Res. **97**, 9669–9688 (1992).
[20]V. I. Karpman, *Nonlinear Waves in Dispersive Media* (Nauka, Moscow, 1973) (in Russian) [English translation: *Nonlinear Waves in Dispersive Media* (Pergamon, Oxford, 1973)].
[21]C. Koop and G. Butler, "An investigation of internal solitary waves in a two-fluid system," J. Fluid Mech. **112**, 225–251 (1981).
[22]H. Segur and J. L. Hammack, "Soliton models of long internal waves," J. Fluid Mech. **118**, 285–304 (1982).
[23]V. I. Bukreev and N. V. Gavrilov, "Experimental investigation of solitary internal waves in a two-layer fluid," Zh. Prikl. Mekh. Tekhn. Fiziki (PMTF) **N.5**, 51–56 (1983) (in Russian) [English translation: Sov. Phys. J. Appl. Mech. Tech. Phys. n.5 (1983)].
[24]K. A. Gorshkov and V. V. Papko, "Non-adiabatic stage of damping of solitons and the intermediate asymptotics," Izv. Vyssh. Uchebn. Zaved., Radiofiz. **20**, 360–365 (1977) (in Russian) [English translation: Radiophys. Quantum Electron. **20**, (1977)].
[25]Ch.-Y. Lee and R. C. Beardsley, "The generation of long nonlinear internal waves in a weakly stratified shear flows," J. Geophys. Res. **79**, 453–457 (1974).
[26]J. Gear and R. Grimshaw, "A second-order theory for solitary waves in shallow fluids," Phys. Fluids **26**, 14–29 (1983).
[27]A. K. Liu, J. R. Holbrook, and J. R. Apel, "Nonlinear internal wave evolution in the Sulu Sea," J. Phys. Oceanogr. **15**, 1613–1624 (1985).
[28]L. Ostrovsky and E. Pelinovsky, "Nonlinear evolution of tsunami waves," Bull. Roy. Soc. New Zealand **15**, 203–211 (1976).
[29]A. R. Osborne, "The inverse scattering transform: tools for the nonlinear Fourier analysis and filtering of ocean surface waves," Chaos, Solitons Fractals **5**, 2623–2637 (1995).
[30]J.-G. Caputo and Y. A. Stepanyants, "Bore Formation, Evolution and Disintegration into Solitons in Shallow Inhomogeneous Channels," Nonlinear Processes Geophys. **10**, 407–424 (2003).
[31]R. Grimshaw, "The solitary wave in water of variable depth," J. Fluid Mech. **42**, 639–656 (1970); "The solitary wave in water of variable depth. Part 2," J. Fluid Mech. **46**, 611–622 (1971).
[32]T. Kakutani and K. Matsuuchi, "Effect of viscosity on long gravity waves," J. Phys. Soc. Jpn. **39**, 237–246 (1975).
[33]J. W. Miles, "Damping of weakly nonlinear shallow-water waves," J. Fluid Mech. **76**, 251–257 (1976).
[34]K. P. Das and J. Chakrabarti, "The Korteweg–de Vries equation modified by viscosity for waves in a two-layer fluid in a channel of arbitrary cross section," Phys. Fluids **29**, 661–666 (1986).
[35]K. R. Helfrich, "Internal solitary wave breaking and run-up on a uniform slope," J. Fluid Mech. **243**, 133–154 (1992).
[36]K. A. Gorshkov and L. A. Ostrovsky, "Interaction of solitons in nonintegrable systems: Direct perturbation method and applications," Physica D **3**, 248–438 (1981).
[37]R. Grimshaw, "Evolution equations for weakly nonlinear long internal waves in a rotating fluid," Stud. Appl. Math. **73**, 1–33 (1985).
[38]D. Renouard and J.-P. Germain, "Experimental study of long nonlinear internal waves in rotating fluid," Ann. Geophys. (Germany) **12**, 254–264 (1994).
[39]L. A. Ostrovsky and Yu. A. Stepanyants, "Nonlinear surface and internal waves in rotating fluids," in *Nonlinear Waves 3*, Proceedings of the 1989 Gorky School on Nonlinear Waves, edited by A. V. Gaponov-Grekhov, M. I. Rabinovich, and J. Engelbrecht (Springer-Verlag, Berlin, Heidelberg, 1990), pp. 106–128. [In Russian: in *Nonlinear Waves. Physics and Astrophysics* (Nauka, Moscow, 1993), pp. 132–153.]
[40]R. H. J. Grimshaw, L. A. Ostrovsky, V. I. Shrira, and Y. A. Stepanyants, "Long nonlinear surface and internal gravity waves in a rotating ocean," Surv. Geophys. **19**, 289–338 (1998).
[41]A. L. New and M. Esteban, "A new Korteweg–de Vries-type theory for internal solitary waves in a rotating continuously-stratified ocean," in *Near-Surface Ocean Layer. V. 1. Physical Processes and Remote Sensing*, Collection of Scientific Papers, edited by E. N. Pelinovsky and V. I. Talanov, Nizhny Novgorod, IAP RAS, 1999, pp. 173–203.
[42]Y. Liu and V. Varlamov, "Stability of solitary waves and weak rotation limit for the Ostrovsky equation," J. Diff. Eqns. **203**, 159–183 (2004).
[43]R. H. J. Grimshaw, J.-M. He, and L. A. Ostrovsky, "Terminal damping of a solitary wave due to radiation in rotational systems," Stud. Appl. Math. **101**, 197–210 (1998).
[44]O. A. Gilman, R. Grimshaw, and Yu. A. Stepanyants, "Dynamics of internal solitary waves in a rotating fluid," Dyn. Atmos. Oceans **23**, 403–411 (1996) (special issue. Stratified flows, Pt. A).
[45]V. O. Vakhnenko, "High-frequency soliton-like waves in a relaxing medium," J. Math. Phys. **40**, 2011–2020 (1999).
[46]Y. Stepanyants, "On stationary solutions of the reduced Ostrovsky equation: periodic waves, compactons and compound solitons," Chaos, Solitons Fractals **28**, 193–204 (2006).
[47]A. I. Leonov, "The effect of Earth rotation on the propagation of weak nonlinear surface and internal long oceanic waves," Ann. N.Y. Acad. Sci. **373**, 150–159 (1981).
[48]V. M. Galkin and Yu. A. Stepanyants, "On the existence of stationary solitary waves in a rotating fluid," Prikl. Mat. Mekh. **55**, 1051–1055 (1991) (in Russian) [English translation: J. Appl. Math. Mech. **55**, 939–943 (1991)].
[49]M. A. Obregon and Yu. A. Stepanyants, "Oblique magneto-acoustic solitons in a rotating plasma," Phys. Lett. A **249**, 315–323 (1998).
[50]O. A. Gilman, R. Grimshaw, and Yu. A. Stepanyants, "Approximate analytical and numerical solutions of the stationary Ostrovsky equation," Stud. Appl. Math. **95**, 115–126 (1995).
[51]T. Gerkema, "A unified model for the generation and fission of internal tides in a rotating ocean," J. Mar. Res. **54**, 421–450 (1996).
[52]R. Plougonven and V. Zeitlin, "On periodic inertia-gravity waves of finite amplitude propagating without change of form at sharp density-gradient interfaces in the rotating fluid," Phys. Lett. A **314**, 140–149 (2003).
[53]Yu. A. Stepanyants, "Experimental investigation of cylindrically diverging solitons in an electric lattice," Wave Motion **3**, 335–341 (1981).
[54]A. A. Dorfman, E. N. Pelinovsky, and Yu. A. Stepanyants, "Finite-amplitude cylindrical and spherical waves in weakly dispersive media," Zhurnal Prikladnoi Mekhaniki i Tekhnicheskoi Fiziki (PMTF) **N.2**, 78–85 (1981) (in Russian) [English translation: Sov. Phys. J. Appl. Mech. Tech.

Phys. **n.2**, 206–211 (1982)].
[55]C. Ramirez, D. Renouard, and Yu. A. Stepanyants, "Propagation of cylindrical waves in a rotating fluid," Fluid Dyn. Res. **30**, 169–196 (2002).
[56]S. V. Iordansky, "Asymptotic behaviour of an axially symmetric diverging wave in a heavy liquid," Dokl. Akad. Nauk SSSR **125**, 1211–1214 (in Russian) (1959) [English translation: Sov. Phys. Dokl. **125**, 6–9 (1959)].
[57]S. Maxon and J. Viecelli, "Cylindrical solitons," Phys. Fluids **17**, 1614–1616 (1974).
[58]F. Calogero and A. Degasperis, "Solution by the spectral-transform method of a nonlinear evolution equation including as a special case the cylindrical KdV equation," Lett. Nuovo Cimento **23**, 150–154 (1978).
[59]A. Nakamura and H. H. Chen, "Soliton solutions of the cylindrical KdV equation," J. Phys. Soc. Jpn. **50**, 711–718 (1981).
[60]C. J. Amick and R. E. L. Turner, "A global theory of internal solitary waves in two-fluid system," Trans. Am. Math. Soc. **298**, 431–484 (1986).
[61]R. E. L. Turner and J.-M. Vanden-Broeck, "Broadening of interfacial solitary waves," Phys. Fluids **31**, 2486–2490 (1988).
[62]W. A. B. Evans and M. J. Ford, "An integral equation approach to internal (2-layer) solitary waves," Phys. Fluids **8**, 2032–2047 (1996).
[63]J. Grue, A. Jensen, P.-O. Rusås, and J. K. Sveen, "Properties of large amplitude internal waves," J. Fluid Mech. **380**, 257–278 (1999).
[64]V. I. Vlasenko and K. Hutter, "Numerical experiments on the breaking of solitary internal waves over a slope-shelf topography," J. Phys. Oceanogr. **32**, 1779–1793 (2002).
[65]V. I. Vlasenko and K. Hutter, "Transformation and disintegration of strongly nonlinear internal waves by topography in stratified lakes," Ann. Geophys. (Germany) **20**, 2087–2013 (2002).
[66]K. G. Lamb, "A numerical investigation of solitary internal waves with trapped cores formed via shoaling," J. Fluid Mech. **451**, 109–144 (2002).
[67]K. G. Lamb, "Shoaling solitary internal waves: on a criterion for the formation of waves with trapped cores," J. Fluid Mech. **478**, 81–100 (2003).
[68]M. Stastna and K. G. Lamb, "Large fully nonlinear internal solitary waves: The effect of background current," Phys. Fluids **14**, 2987–2999 (2002).
[69]G. B. Whitham, "Variational methods and applications to water waves," Proc. R. Soc. London, Ser. A **299**, 6–25 (1967).
[70]M. Miyata, "An internal solitary wave of large amplitude," La Mer **23**, 43–48 (1985).
[71]M. Miyata, "Long internal waves of large amplitude," in *Nonlinear Water Waves*, edited by K. Horikawa and H. Maruo (Springer-Verlag, Berlin, 1988), pp. 399–406.
[72]M. Miyata, "A note on broad narrow solitary waves," IPRC Report 00-01, SOEST, University of Hawaii, Honolulu, 00-05, 2000, p. 47.
[73]H. Michallet and E. Barthélemy, "Experimental study of interfacial solitary waves," J. Fluid Mech. **366**, 159–177 (1998).
[74]W. Choi and R. Camassa, "Fully nonlinear internal waves in a two-fluid system," J. Fluid Mech. **386**, 1–36 (1999).
[75]L. A. Ostrovsky and J. Grue, "Evolution equations for strongly nonlinear internal waves," Phys. Fluids **15**, 2934–2948 (2003).
[76]L. A. Ostrovsky, in The 1998 WHOI/IOS/ONR Internal Solitary Wave Workshop: Contributed Papers, edited by T. F. Duda and D. M. Farmer, Technical Report, WHOI 99-07, 1999, pp. 224–229.
[77]A. V. Slunyaev, E. N. Pelinovsky, O. E. Poloukhina, and S. L. Gavrilyuk, "The Gardner equation as the model for long internal waves," in *Topical Problems of Nonlinear Wave Physics*, Proceedings of the International Symposium, Inst. of Appl. Phys., RAS, Nizhny Novgorod, 2003, pp. 368–369.
[78]S. M. Khasanov, "The propagation of Kelvin's solitary waves in an absorbing medium," Izv. Akad. Nauk SSSR, Fiz. Atmos. Okeana **25**, 307–311, 1989 (in Russian) [English translation: Izv., Acad. Sci., USSR, Atmos. Oceanic Phys. **25**, 3–6 (1989)].
[79]G. H. Keulegan, "Gradual damping of solitary waves," J. Res. Natl. Bur. Stand. **40**, 480–487 (1948).
[80]N. V. Gavrilov, "Internal solitary waves of large amplitude in a two-layer fluid," Zh. Prikl. Mekh. i Tekhn. Fiziki (PMTF) **N.5**, 49–54 (1986) (in Russian) [English translation: Sov. Phys. J. Appl. Mech. Tech. Phys. n.5 (1986)].
[81]L. V. Ovsyannikov *et al.*, *Nonlinear Problems of the Theory of Surface and Internal Waves* (Nauka, Novosibirsk, 1985), in Russian.
[82]V. V. Papko (private communication).
[83]T. Gerkema and J. T. F. Zimmerman, "Generation of nonlinear internal tides and solitary waves," J. Phys. Oceanogr. **25**, 1081–1094 (1995).
[84]A. P. Stamp and M. Jacka, "Deep-water internal solitary waves," J. Fluid Mech. **305**, 347–371 (1995).
[85]D. I. Pullin and R. H. J. Grimshaw, "Large-amplitude solitary waves at the interface between two homogeneous fluids," Phys. Fluids **31**, 3550–3559 (1988).
[86]K. K. Tung, T. F. Chan, and T. Kubota, "Large amplitude internal wave of permanent form," Stud. Appl. Math. **66**, 1–44 (1982).
[87]B. Turkington, A. Eydeland, and S. Wang, "A computational model for solitary internal waves in a continuously stratified fluid," Stud. Appl. Math. **85**, 93–104 (1991).
[88]J. Grue, A. Jensen, P.-O. Rusås, and J. K. Sveen, "Breaking and broadening of internal solitary waves," J. Fluid Mech. **413**, 181–217 (2000).
[89]W. K. Melville and K. R. Helfrich, "Transcritical two-layer flow over topography," J. Fluid Mech. **178**, 31–52 (1987).
[90]J. Grue, A. Fris, E. Palm, and P. O. Rusås, "A method for computing unsteady fully nonlinear interfacial waves," J. Fluid Mech. **351**, 223–252 (1997).
[91]T. Maxworthy, "A note on the internal solitary waves produced by tidal flow over a three-dimensional ridge," J. Geophys. Res. **84**, 338–346 (1979).
[92]J. K. Sveen, Y. Guo, P. Davies, and J. Grue, "On the breaking of internal waves at a ridge," J. Fluid Mech. **469**, 161–188 (2002).
[93]J. Grue, "Generation, propagation and breaking of internal solitons," Chaos **15**, 037110 (2005).
[94]R. Grimshaw "Adjustment processes and radiating solitary waves in a regularised Ostrovsky equation," Eur. J. Mech. B/Fluids **18**, 535–543 (1999).
[95]E. J. Parkes, "Explicit solutions of the reduced Ostrovsky equation" (in press).